The denitrosylase SCoR2 controls cardioprotective metabolic reprogramming

Zachary W. Grimmett[1,2], Rongli Zhang[2,3], Hua-Lin Zhou[2], Qiuying Chen[4], Dawson Miller[4], Zhaoxia Qian[2], Justin Lin[2], Riti Kalra[2], Steven S. Gross[4], Walter J. Koch[5,6], Richard T. Premont[2,7], Jonathan S. Stamler[2,7,*]

[1] Medical Scientist Training Program, Case Western Reserve University School of Medicine, Cleveland OH, 44106

[2] Institute for Transformative Molecular Medicine, Department of Medicine, Case Western Reserve University School of Medicine, Cleveland OH, 44106

[3] Cardiovascular Research Institute, Case Western Reserve University School of Medicine, Cleveland OH, 44106

[4] Department of Pharmacology, Weill Cornell Medicine, New York, NY, 10065

[5] Department of Surgery, Duke University School of Medicine, Durham NC, 27710

[6] Department of Medicine, Duke University School of Medicine, Durham NC, 27710

[7] Harrington Discovery Institute, University Hospitals Cleveland Medical Center, Cleveland OH, 44106

[*] Corresponding Author, jss156@case.edu

ABSTRACT

Acute myocardial infarction (MI) is a leading cause of morbidity and mortality, and therapeutic options remain limited. Endogenously generated nitric oxide (NO) is highly cardioprotective, but protection is not replicated by nitroso-vasodilators (e.g., nitrates, nitroprusside) used in clinical practice, highlighting specificity in NO-based signaling and untapped therapeutic potential. Signaling by NO is mediated largely by S-nitrosylation, entailing specific enzymes that form and degrade S-nitrosothiols in proteins (SNO-proteins), termed nitrosylases and denitrosylases, respectively. SNO-CoA Reductase 2 (SCoR2; product of the *Akr1a1* gene) is a recently discovered protein denitrosylase. Genetic variants in SCoR2 have been associated with cardiovascular disease, but its function is unknown. Here we show that mice lacking SCoR2 exhibit robust protection in an animal model of MI. SCoR2 regulates ketolytic energy availability, antioxidant levels and polyol homeostasis via S-nitrosylation of key metabolic effectors. Human cardiomyopathy shows reduced SCoR2 expression and an S-nitrosylation signature of metabolic reprogramming, mirroring SCoR2$^{-/-}$ mice. Deletion of SCoR2 thus coordinately reprograms multiple metabolic pathways—ketone body utilization, glycolysis, pentose phosphate shunt and polyol metabolism—to limit infarct size, establishing SCoR2 as a novel regulator in the injured myocardium and a potential drug target.

Impact statement: Mice lacking the denitrosylase enzyme SCoR2/AKR1A1 demonstrate robust cardioprotection resulting from reprogramming of multiple metabolic pathways, revealing widespread, coordinated metabolic regulation by SCoR2.

INTRODUCTION

Cardiovascular disease resulting in myocardial infarction (MI) is the leading cause of death in the U.S. (*1*). In the setting of an acute MI, preservation of even an additional 5% of myocardial tissue can reduce mortality and progression to heart failure (*2*). However, despite decades of research, no FDA-approved drug can reduce infarct size, and post-MI morbidity/mortality remains high (*3*). Targeting well-described mediators of myocardial ischemia-reperfusion (I/R) injury, such as intracellular Ca^{2+} overload, pH imbalance, oxidative stress, and inflammation, has thus far been unsuccessful in mitigating lethal cardiac injury in humans (*4–6*).

An extensive literature spanning over 3 decades details the protective effects of nitric oxide (NO) in myocardial ischemia (*7–14*), including regulation of mitochondrial energetics, Ca^{2+} transport, HIF-1α-mediated hypoxia response, and cytoprotection. It is increasingly appreciated that NO signals largely through protein S-nitrosylation (*15*), a ubiquitous post-translational modification that regulates protein conformation or activity with manifold functional consequences. S-nitrosylation has been convincingly demonstrated to exert a broadly protective role in myocardial I/R injury (*10*,*14*). Accumulating evidence implicates specific enzymes that attach (nitrosylases) and remove (denitrosylases) NO groups at target Cys residues (*15–17*), by direct analogy to kinases and phosphatases that add and remove phosphate groups (i.e. phosphorylation). Studies of the founding member of the denitrosylase family, S-nitrosoglutathione (GSNO) reductase (GSNOR), have identified important roles in ischemia-reperfusion (I/R) and transverse aortic constriction (TAC) models of cardiac injury in mice, and in cardiac arrest in humans (*18*). Targets of GSNOR include SNO-HIF-1α (*10*), SNO-ANT1 (*19*), and SNO-GRK2 (*20*,*21*), suggesting GSNOR confers protection through multiple synergistic mechanisms.

SCoR2 (AKR1A1) is a newly identified protein denitrosylase with distinct cellular distribution, substrates, and purview (*22*,*23*); it is mechanistically and functionally homologous to yeast SCoR1/Adh6 (*22*). SCoR2 is highly expressed in kidney proximal tubules, but also found at low levels in other tissues including the heart (*24*). Inhibition of SCoR2 by genetic knockout or drug treatment protects mice from acute kidney injury (*24*,*25*) and lowers cholesterol by inhibiting liver PCSK9 secretion (*26*). SCoR2 acts on seemingly distinct sets of SNO-protein substrates in the kidney and liver suggesting that its broader role in biology remains to be understood. Genetic variants in SCoR2/AKR1A1 are associated with heart failure (*27–29*) and cardiovascular function in humans (*30*,*31*); however, the role and function of SCoR2 in the cardiovascular system remains unexplored. We therefore assessed cardiac protection in mice lacking SCoR2 and employed a multi-omic approach to define SCoR2-dependent protective changes following cardiac ischemia/reperfusion injury.

RESULTS

Cardiovascular physiology of SCoR2

Measures of cardiac function by echocardiography were unchanged at baseline in SCoR2$^{-/-}$ mice relative to SCoR2$^{+/+}$, including ejection fraction, fractional shortening, left ventricular internal diameter at end-systole (LVID-s), and ventricular pressures (Fig. S1A-F). SCoR2$^{-/-}$ mice also did not differ in blood pressure (Fig. S1G, H), heart rate (Fig. S1I), body weight (Fig. S1J), or heart/lung weight (Fig. S1K). Thus, knockout of SCoR2 has no major effect on baseline cardiac function.

SCoR2$^{-/-}$-mediated cardioprotection in an animal model of MI

We employed a model of acute MI, in which the left anterior descending artery (LAD) is ligated for 30 min, followed by 1-24 hr of reperfusion. LAD ligation induced ST-elevation, confirmed by electrocardiography (EKG), characteristic of acute myocardial ischemia. Mice lacking SCoR2 exhibited markedly reduced infarct size after ischemia/reperfusion (I/R) injury, as measured by differential Evans blue/TTC staining of left ventricle (LV) cross-sections distal to the ligation (Fig. 1A). Area of necrosis (AON) as a percentage of total LV area and as a percentage of area at risk (AAR) were also decreased in SCoR2$^{-/-}$ mice relative to SCoR2$^{+/+}$ mice, though AAR/LV was not different (Fig. 1B). Thus, SCoR2 deletion is protective in I/R injury, implying that its denitrosylated substrates contribute to tissue damage.

Cardiac function was assessed by transthoracic echocardiography 24 hours after I/R injury. Ejection fraction (EF) and fractional shortening (FS) were both better maintained in SCoR2$^{-/-}$ mice relative to SCoR2$^{+/+}$ (Fig. 1C). LVID-s was reduced in SCoR2$^{-/-}$ hearts vs. SCoR2$^{+/+}$ (Fig. 1D), consistent with preserved LV function. Heart rate, stroke volume and cardiac output remained unchanged in SCoR2$^{-/-}$ mice relative to SCoR2$^{+/+}$ (Fig. S1L-N), and markers of cardiac hypertrophy (LV posterior wall (LVPW) and interventricular septum (IVS) thickness) were also unchanged (Fig. S1O-R). Cardiac troponin-1 released into the bloodstream at 4hr after LAD ligation was reduced by SCoR2 deletion (Fig. 1E). Likewise, lactate dehydrogenase (LDH) levels in plasma were lower in injured SCoR2$^{-/-}$ mice compared to SCoR2$^{+/+}$ at 4 hr post-reperfusion (Fig. 1F). Notably, SCoR2$^{-/-}$ mice demonstrated improved post-MI survival (12/30; 40%) relative to SCoR2$^{+/+}$ mice (5/27; 19%) at 4 hours post-reperfusion, supportive of an acute cardioprotective phenotype (Fig. 1G). Fewer TUNEL^{+} nuclei were observed in the myocardium of SCoR2$^{-/-}$ mice at 4 hr post-MI, indicating reduced apoptotic cell death (Fig. 1H, I).

SCoR2 mediates denitrosylation of cardiac SNO-proteins

The canonical NO-stimulated cGMP/protein kinase G pathway protects against cardiac injury (*32*), but cGMP levels after I/R were no different in SCoR2$^{+/+}$ vs. SCoR2$^{-/-}$ mice (Fig. 2A), suggesting protection mediated by protein S-nitrosylation (*33*,*34*) (Fig. S2A). Indeed, while SCoR2 expression was verified in WT heart (Fig. S2B), its activity was eliminated in hearts from SCoR2$^{-/-}$ mice (Fig. S2C), and protein S-nitrosylation was elevated at baseline (i.e., in the uninjured SCoR2$^{-/-}$ mouse heart) (Fig. S2D,E). Further, in SCoR2$^{+/+}$ heart lysates at baseline, addition of SNO-CoA (SCoR2 substrate and NO donor (*35*)) alone increased protein S-nitrosylation (Fig. 2B), whereas co-administration of NADPH (the electron donor used by SCoR2 during denitrosylation) led to a decrease in cardiac SNO-proteins (Fig. 2C, D). Although other denitrosylase enzymes are present in the heart, SCoR2 is responsible for approximately 65% of NADPH-dependent denitrosylase activity (Fig. S2C); thus, SCoR2 regulates protein S-nitrosylation in the heart. Conversely, while SCoR2/AKR1A1 is required for vitamin C synthesis (*36*), mice were supplemented with vitamin C, and other putative carbohydrate substrates for SCoR2 /aldo-keto reductase activity were undetectable (Table S2).

Multi-omic analysis identifies SCoR2-regulated cardioprotective pathways

To identify proteins whose S-nitrosylation was regulated by SCoR2 following cardiac injury, heart lysates from SCoR2$^{+/+}$ vs. SCoR2$^{-/-}$ mice at 4 hr post-I/R (vs. sham) were subjected to SNORAC and visualized by staining with Coomassie blue (Fig. 3A). To elucidate mechanisms of SCoR2 deficiency-dependent cardioprotection and identify sites of regulation, we subjected post-I/R SCoR2$^{+/+}$ and SCoR2$^{-/-}$ mouse hearts to three complementary unbiased screens (done in triplicate): 1. SCoR2-dependent nitrosoproteome; 2. SCoR2 interactome; 3. SCoR2-dependent metabolome (heart and plasma) (Fig. 3B).

LC-MS/MS of SNORAC samples from 4 hr post-I/R SCoR2$^{+/+}$ and SCoR2$^{-/-}$ mouse heart identified nearly 2000 unique SNO-proteins. Of these, 158 proteins showed increased S-nitrosylation (>1.2 fold) in post-I/R SCoR2$^{-/-}$ hearts relative to post-I/R SCoR2$^{+/+}$, comprising the SCoR2-dependent nitrosoproteome (Fig. 3B, Table S1). Notably, metabolic proteins are heavily represented in the cardiac SCoR2-dependent nitrosoproteome (35/158 proteins; Table S1), similar to wild-type hearts (*37*).

Co-immunoprecipitation using anti-SCoR2 antibody in untreated SCoR2$^{+/+}$ heart lysate coupled with LC-MS/MS identified 515 SCoR2-associated proteins (SCoR2-dependent interactome) (Fig. 3B; Table S1), of which 31 overlapped the SCoR2-dependent nitrosoproteome (Fig. 3B, C). Since these 31 SNO-proteins both associated with SCoR2 and displayed SCoR2-dependent S-nitrosylation, they represent candidate SCoR2 denitrosylation substrates.

Untargeted metabolite profiling (using an LC/MS metabolomic platform) was performed using heart lysate and blood plasma from 4 hr post-I/R SCoR2$^{+/+}$ and SCoR2$^{-/-}$ mice to identify metabolites that may be regulated by SCoR2-dependent SNO-proteins (SCoR2-dependent metabolome) (Table S2). These metabolite studies identified three metabolic pathways that were significantly perturbed by SCoR2 deletion: ketone body oxidation, pentose phosphate pathway (PPP), and polyol metabolism.

Finally, multi-omic analysis by integration of all this data identified two specific SCoR2-substrate SNO-proteins, β-hydroxybutyrate dehydrogenase (BDH1) and pyruvate kinase M2 (PKM2) (Fig. 3B, C). This unbiased analysis suggests that these two enzymes are likely to be key contributors

to metabolic reprogramming after cardiac I/R, identifying specific targets for SCoR2 in its regulation of cardiac metabolism.

SCoR2 regulates ketolytic energy availability through BDH1 stability

BDH1 catalyzes the first step of ketone body breakdown in the heart, the oxidation of β-hydroxybutyrate (BHB) to acetoacetate, allowing cardiac muscle cells to use ketone bodies as an alternative source of energy in the absence of glucose and/or fatty acids (*38*,*39*). Cardiac-specific BDH1 overexpression is known to be protective in mice subjected to cardiac injury, attributed to increased cardiac ketone body oxidation and associated increase in antioxidant defenses (*40*).

S-nitrosylation of BDH1 has been reported in proteomic screens (*41*) but remains entirely uncharacterized. In the post-I/R heart, we confirmed that SNO-BDH1 was increased in SCoR2$^{-/-}$ mice relative to SCoR2$^{+/+}$ (Fig. 4A, quantified from Western blots in Fig. S3A). Notably, total BDH1 protein expression was also increased in SCoR2$^{-/-}$ mice 4 hr after injury (Fig. 4B, quantified from Western blots in Fig. S3A), suggesting that SCoR2-controlled S-nitrosylation may regulate BDH1 stability. Indeed, the ratio of SNO-BDH1 to total BDH1 was not different in SCoR2$^{-/-}$ heart relative to SCoR2$^{+/+}$ (Fig. 4C). Such regulation of SNO-BDH1 by SCoR2 appears specific to the heart, as levels of SNO-BDH1 and BDH1 were unchanged in post-I/R SCoR2$^{+/+}$ vs. SCoR2$^{-/-}$ liver (Fig. 4D-F, quantified from Western blots in Fig. S3B). To assess effects of S-nitrosylation on BDH1 stability, we first identified the predominant site of SNO modification as Cys^{115} (out of 7 total Cys residues), since in vitro SNO-CoA treatment failed to increase SNO-BDH1 in the Cys115Ser (C115S) mutant relative to WT BDH1 (Fig. 4G). We next assessed BDH1 stability using a pulse-chase assay with the translation inhibitor cycloheximide (CHX chase) to measure the rate of BDH1 protein degradation in HEK293 cells. WT BDH1 protein expression decreased

steadily over 12-24 hours (Fig. 4H; black bars), while addition of a cell permeant NO donor (ethyl ester CysNO, ECNO) markedly increased BDH1 stability (pink bars). This stabilizing effect of NO was lost upon mutation of Cys^{115} in BDH1 (Fig. 4H; blue and purple bars, quantified as area under the curve in Fig. 4I, with a representative Western blot in Fig. S3C), validating SNO-mediated stabilization of BDH1 and localizing the primary effect of NO to this single Cys residue.

We next sought the effects of SNO-BDH1 that might contribute to cardioprotection. We observed that acetoacetic acid, the ketone body produced by BDH1 in the heart, remained elevated in the plasma of $SCoR2^{-/-}$ mice after injury (Fig. 4J), while acetoacetate level in the heart and BHB level in heart and plasma remained relatively unchanged between $SCoR2^{+/+}$ and $SCoR2^{-/-}$ (Fig. 4K, Fig. S3D,E). Metabolism of ketone bodies produces acetyl-CoA as an energetic intermediate, and we observed an increase in acetyl-CoA in hearts from $SCoR2^{-/-}$ mice (Fig. 4L). Energy in the form of acetyl-CoA is used for ATP production, and excess ATP energy can be stored in muscle tissue as phosphocreatine (p-Cr). At the sarcoplasmic reticulum, p-Cr can be used rapidly to synthesize ATP in energy-starved states such as ischemia, supplying ATP for continued myocardial contraction, which is cardioprotective (*42*). In the injured $SCoR2^{-/-}$ heart, we observed dramatically increased stored energy availability in the form of p-Cr, relative to $SCoR2^{+/+}$ at 4 hr post-I/R (Fig. 4M). Together, these data support a role for increased energy availability in cardioprotection of $SCoR2^{-/-}$ mice after I/R injury (summarized in the model shown in Fig. 4N).

<u>Regulated S-nitrosylation by SCoR2 in human hearts</u>

BDH1 Cys^{115} is conserved in mammals (Fig. S3F), suggesting critical function. We therefore sought confirmation of a role for SNO-BDH1 in humans. S-nitrosylation of BDH1 was detected in human heart tissue and SNO-BDH1 was elevated in hearts from patients with non-ischemic

cardiomyopathy (NICM) (Fig. 4O, representative image; quantified in Fig. 4P). We reasoned that S-nitrosylation of BDH1 may be regulated by SCoR2 in humans. Expression of SCoR2 was in fact decreased in heart tissue from patients with NICM relative to healthy human heart tissue (Fig. 4Q, R), suggesting an inverse relationship between SCoR2 activity and SNO-BDH1 levels, as seen in mice.

Interestingly, in patients with ischemic cardiomyopathy (ICM), SNO-BDH1 was decreased and SCoR2 levels were preserved, indicating context-specific regulation (and possibly maladaptive change; Fig. 4S,T, representative SNORAC/Western blot in Fig. S3G,H). Most importantly, we observed a significant correlation between SNO-BDH1 and total BDH1 (Fig. 4U), suggesting S-nitrosylation may enhance BDH1 stability in human heart tissue, supporting our findings in cell culture (Fig. 4H,I). Altogether, our data demonstrate that S-nitrosylation of metabolic proteins may correlate with human disease, suggests that SNO-BDH1 may be a protective locus that is regulated by SCoR2, and identifies a possible signature of SCoR2 deficiency in human NICM.

SCoR2 regulates glycolytic and PPP intermediates through S-nitrosylation of PKM2

PKM2 is the injury-upregulated splice variant of muscle-type pyruvate kinase, which includes a regulatory SNO-site controlling PKM2 conversion of phosphoenolpyruvate to pyruvate in glycolysis. S-nitrosylation of PKM2 at $Cys^{423/424}$ inhibits glycolytic flux, thereby shunting glycolytic intermediates into the PPP (*33*,*43*) to produce antioxidants (NADPH) and nucleotide precursors. The PPP can also generate newly identified polyol precursors subject to additional SCoR2 regulation, as detailed below. PKM2 is upregulated by ischemic injury and SNO-PKM2 is known to be protective in the context of ischemia in the kidney (*33*) and oxidative stress in the endothelium (*43*). Notably, hearts of patients with ICM showed a significant increase in SNO-

PKM2 (Fig. 5A; representative SNORAC and Western blot in Fig. S3G,H), consistent with a cardioprotective effect.

In 4 hr post-I/R heart, the level of lactate, a product of inefficient glycolysis during ischemia that is associated with worse clinical outcomes in patients with MI (*44*), is markedly reduced (Fig. 5B), suggesting reduced activity of the glycolysis pathway. More directly, we observed increased glycolytic and non-glycolytic input into the PPP in SCoR2$^{-/-}$ heart (Table 1), including plasma pyruvate (Fig. 5C) and arabinose (Fig. 5D). Pyruvate is produced through multiple metabolic pathways, including non-glycolytic pathways, and can enter the PPP through conversion to xylose. Together, these findings indicate that metabolites available to the PPP are increased in the absence of SCoR2, consistent with inhibition of SNO-PKM2 (Fig. 3B) (as observed in multiple tissues (*33*,*43*) and known to be protective in the setting of ischemia (*24*)). We also observed that products of the PPP are increased in SCoR2$^{-/-}$ heart, including NADPH (Fig. 5E) and erythrose 4-phosphate (Fig. 5F), as well as increased ribose (Fig. 5G) and deoxyribose (Fig. 5H) in SCoR2$^{-/-}$ plasma. Altogether, this metabolic signature is consistent with the previously described inhibition of PKM2 by S-nitrosylation in the absence of SCoR2 (*33*).

<u>SCoR2 regulates endogenous production of harmful polyol compounds</u>

Regulation of polyol metabolism by SCoR2 may contribute to protection from myocardial ischemia. Elevated levels of polyols, organic metabolites with > 1 hydroxyl group, have recently been associated with short-term (< 3 year) risk for major adverse cardiovascular events (*45*,*46*). We observed that two polyols, arabitol/ribitol and sorbitol, were markedly decreased in plasma from SCoR2$^{-/-}$ mice relative to SCoR2$^{+/+}$ (Fig. 5I,J). Additionally, plasma levels of each polyol

rose at 4 hours post-I/R relative to sham or 1hr post-I/R in SCoR2$^{+/+}$ mice, but not in SCoR2$^{-/-}$ mice.

Endogenous polyol production remains relatively uncharacterized in humans. Some polyols may derive from PPP metabolites (xylulose, ribulose, ribose, erythrose, etc.) (*47*,*48*) via actions of multiple reductase enzymes (*49*), but rigorous evidence is lacking. To test whether SCoR2 might directly generate polyols that we find to be elevated in the absence of SCoR2 (arabitol/ribitol, sorbitol; Fig. 5I,J), we measured reduction of the corresponding carbohydrates (i.e., arabinose, ribose, glucose, and fructose) in the presence of recombinant SCoR2 (vs. the canonical SCoR2 substrate SNO-CoA as positive control). Using multiple carbohydrates known or predicted to form polyols upon reduction as potential substrates, SCoR2 demonstrated no direct reductase activity as measured by NADPH consumption (Fig. 5K). The related enzyme AKR1B1 can reduce glucose to the polyol sorbitol, but glucose is not a good substrate for AKR1A1/SCoR2 (*50*,*51*) and was not reduced in our assay (Fig. 5K).

Alternative substrates of SCoR2 in polyol metabolism

SCoR2 has been formally classified as an aldoketoreductase. However, putative carbonyl substrates of SCoR2/AKR1A1 have not been validated in situ and were not detectable in SCoR2$^{-/-}$ heart or plasma (Table S2). These data are consistent with SCoR2 functioning primarily as a denitrosylase to regulate polyol metabolism via multiple enzymes, rather than as a direct carbohydrate reductase. Indeed, multiple reductase enzymes were identified in the SCoR2-dependent nitrosoproteome (e.g., ALDH1B1 and DHRS7B, Table S1), some of which may catalyze direct reduction of carbohydrates to polyols in an S-nitrosylation- and SCoR2-dependent manner. Multiple reductase and aldolase enzymes were recently identified as interacting partners

with polyols (such as arabitol) and related carbohydrates (such as arabinose, ribulose, xylose, ribose, and xylulose) (*52*), including aldolase B, MDH2, PDH, and IDH3. All have been identified in SNO-proteomic screens (*53*) and may also be SCoR2-regulated. Taken together, our findings lead to an overall model (Fig. 5L) in which SCoR2 reprograms cardiac metabolism through multiple metabolic pathways including cardiac ketolysis, glycolysis, PPP, and polyol metabolism, to increase protective NADPH and phosphocreatine in the mouse heart, while decreasing lactate and multiple polyols that are associated with poor cardiovascular outcomes.

DISCUSSION

The cardioprotective role of NO in pre-clinical models of acute MI is well established (*11–13*,*54*). However, the ability of NO donors to reduce I/R damage has been disappointing in the clinical setting (*55*,*56*). One explanation for these failures is the absence of protein targets or cardioprotective mechanisms by which to assess efficacy of NO donor drugs. This challenge is circumvented through enzymatically regulated S-nitrosylation, where the target has been genetically validated. In particular, the denitrosylase SCoR2 (*22*) regulates multiple metabolic pathways, including ketolysis, glycolysis, PPP, and polyol metabolism, that have established roles in cardioprotection, but were not previously known to be coordinately regulated. Our studies thus identify a comprehensive role for SCoR2 in regulating cardiac metabolism and suggest a new approach to cardioprotection through global metabolic reprogramming vis-à-vis SCoR2-dependent protein S-nitrosylation.

A large body of evidence supports the benefits of ketones in acute myocardial injury. BDH1 catalyzes the initial step in the breakdown of the ketone BHB in extrahepatic tissues, and cardiac-specific knockout of BDH1 in mice leads to more severe ventricular dysfunction following

ischemia (*57*). Conversely, cardiac-specific BDH1 overexpression improves contractile function in response to injury (*40*). Ketone bodies secreted from the liver are a critical source of myocardial energy during fasting (*58–60*) and also in the failing (*38*,*39*) and ischemic heart (*61*), where they reduce infarct size and improve post-I/R contractile function (*62–64*). Exogenous BHB reduces infarct size in rats (*65*) and mice (*66*) subjected to I/R injury by increasing ATP production, and is beneficial in patients with cardiogenic shock (*67*), providing evidence that ketolysis contributes to superior metabolism that is beneficial in the setting of acute I/R injury. Circulating ketone bodies are elevated in humans with congestive heart failure (*68*) and are associated with improved cardiac function (*69*) and a lower risk of adverse events in acute MI (*70*). Cardiac ketone body metabolism, beginning with BDH1-mediated breakdown of BHB, is thus a validated protective pathway in acute I/R injury and is beneficial in the context of human cardiovascular disease.

In this context, we have discovered that SCoR2 regulates S-nitrosylation of cardiac BDH1 at Cys^{115} thereby governing its stability. BDH1 expression is thus increased in $SCoR2^{-/-}$ hearts, in accord with its increased S-nitrosylation. Increased expression of BDH1 increases capacity for ketolysis, improving energy reserves (i.e., p-Cr) during ischemia (*71*), as we confirm here. Many studies, including over 40 controlled trials in patients with CAD, HF, or cardiac surgery (*42*), have demonstrated that p-Cr is cardioprotective (*42*,*72–76*), an effect attributed to increased energy availability. Strategies to increase p-Cr in the post-ischemic myocardium are thus a promising avenue to reduce post-MI tissue damage. In this light, we show that inhibition of SCoR2 results in increased p-Cr.

PKM2 is a pyruvate kinase splice variant expressed in development, injury, and cancer (*77*,*78*). PKM2 inhibition is strongly linked to tissue protection, regeneration, and repair (*33*,*43*,*79*,*80*),

including in the heart where inhibition (*80*) or genetic deletion (*79*) leads to reduced infarct size. S-nitrosylation of PKM2 inhibits activity and thus progression of intermediates through glycolysis (*33*); instead glucose 6-phosphate is shunted into the PPP, where it is used to synthesize the antioxidant NADPH and 5-carbon sugars for biosynthesis (*81*). This is protective in the setting of MI (*82*,*83*). The PPP is responsible for producing a portion of the cardiac NADPH pool, and this pathway is upregulated in stressed or injured cardiac tissue (*84–86*). SNO-PKM2, a validated SCoR2 substrate, protects against ischemic kidney injury (*33*) and endothelial damage (*43*) via increased flux through the PPP shunt (*33*,*87*). We demonstrate that deletion of SCoR2 leads to an increase in SNO-PKM2 in the heart, accompanied by inhibition of glycolysis (decreased lactate) and stimulation of the PPP (increased NADPH, erythrose 4-phosphate and ribose). We also observe an increase in other inputs into the PPP (primarily those converging on xylulose, such as galactaric acid, xylose, and lyxose, among others), supporting a comprehensive role for SCoR2 in regulation of the protective PPP shunt in the context of acute ischemic injury.

Polyols are relatively understudied organic metabolites containing more than 1 hydroxyl group. The "polyol pathway" historically refers specifically to sorbitol (*88*); however, there are many other polyols that are metabolically relevant, and indeed other polyols were first described in mammals in the mid-20th century (*89*,*90*). Endogenous production of polyols, well characterized in microorganisms such as lactic acid bacteria (*Lactobacillus, E. avium, L. casei,* and others) (*91*,*92*), has remained underappreciated and relatively uncharacterized in humans. Recent evidence of endogenous erythritol synthesis in human blood (*93*), and in A549 lung cancer cells by the reductases ADH and SORD (*94*), casts doubt on the view that polyols are not endogenously produced in humans (*95*). Additionally, heritable genetic mutations (i.e., in transketolase (*96*), transaldolase (*97*), and ribose-5-phosphate isomerase (*48*)) may lead to aberrant accumulation of

certain polyols (ribitol, arabitol, and erythritol), suggesting close connections to the PPP. Many polyols are structurally related to PPP intermediates, such as arabitol, xylitol, and ribitol, and are likely derived at least in part from these compounds (*47*,*48*). Most studies appear to presume that any polyols produced are simply excreted from the body (*96*).

However, there is tantalizing new evidence that polyols impact cardiovascular health (*45*,*46*). Erythritol, xylitol, threitol, arabitol, and myo-inositol are highly associated with incident risk for major adverse cardiovascular events, and erythritol, in particular, is reported to enhance in vitro platelet reactivity and in vivo thrombosis rate (*45*). Our untargeted metabolomic analysis revealed that SCoR2 deletion causes a marked reduction in these polyol "off-shoots" from the PPP, particularly arabitol/ribitol (indistinguishable in our analysis) and sorbitol, a difference that widens after 4 hours of reperfusion relative to sham injury. We present strong evidence that this effect is not mediated through direct reduction of carbohydrates by SCoR2, in contrast with a recent study (where the actual data are negative (*98*), supporting our findings) and literature viewpoint. Rather, the many observed changes in carbohydrates and corresponding polyols are seemingly well rationalized by the widespread alterations in S-nitrosylation of metabolic enzymes (Table S1) accompanying SCoR2 deletion. Reduction in polyol levels thus represents a fourth SCoR2-regulated metabolic pathway contributing to comprehensive metabolic reprogramming during I/R injury.

The concept that protein S-nitrosylation can be regulated independently of NO synthesis changes the therapeutic paradigm in myocardial ischemia. Protein denitrosylases, including both GSNOR (*10*,*19*,*99–101*) and thioredoxin (*102*,*103*), have been shown to play important roles in cardiac injury and repair. However, a general framework for how these enzymes confer protection has

been missing. Here we establish such a framework for SCoR2 through metabolic regulation, whereby it coordinately orchestrates multiple metabolic pathways for therapeutic gain. These findings help to cement SCoR2 as a major regulator of metabolism in the injured myocardium, and a new class of pharmaceutical target in myocardial ischemia.

Limitations

The results presented here are purposefully limited to the acute response to cardiac tissue injury, and do not explore whether deletion or inhibition of SCoR2 may be beneficial in long-term recovery from MI. We expect that metabolic regulation in chronic injury may involve additional pathways. The protection offered by SCoR2-mediated metabolic reprogramming is also specific to MI injury, although suggestive findings are shown in human cardiomyopathy. We identified the critical enzymes PKM2 and BDH1 via unbiased multi-omic screens, and we surmise they coordinately regulate increased flux through the PPP and ketolysis pathways upon function-regulating S-nitrosylation thereby explaining improved energy balance, but this supposition will benefit from further direct metabolic flux analysis or similar experiments.

MATERIALS AND METHODS

Cell lines

HEK293 cells (ATCC CRL-1573) were obtained from ATCC and cultured in Dulbecco's modified Eagle's medium (DMEM) containing 10% fetal bovine serum and antibiotic/antimycotic solution (Gibco™ 15240096) (complete DMEM). All cells were grown at 37°C under 5% CO_2.

Plasmid construction and mutagenesis

The BDH1 (human) cDNA in pDONR223 entry vector was obtained from DNAsu (clone:HsCD00352477). This entry vector was cloned into Gateway pcDNA-DEST40 (mammalian expression, under CMV promoter; cat#43-0101; Invitrogen) with V5 epitope tag, using Gateway LR Clonase II (cat#11791-020; Invitrogen) enzyme reaction, and the LR reaction was transformed into One Shot Omnima cells (cat# C8540-03; Invitrogen) and streaked onto selective Amp+ plates. A single colony was isolated, expanded in LB+Amp media, and plasmid purified by Qiagen Plasmid Maxi Kit (cat#12362; Qiagen). The resulting plasmid was sequenced to confirm correct gene and vector sequence. C115S-BDH1 mutant was generated using QuikChange II Site-Directed Mutagenesis Kit (cat# 200523; Agilent) using mutagenesis primers (forward: 5'-CGTCCAGCTCAATGTCTCCAGCAGCGAAGAGG; reverse: 5'-CCTCTTCGCTGCTGGAGACATTGAGCTGGACG) from Invitrogen. Empty vector (pcDNA3.1(+); Invitrogen) was expanded and sequenced as described above.

Transfection

For BDH1 transfections, HEK293 cells were plated onto dishes coated with 5mg/cm^2 poly-D-lysine (Corning) and cultured for 24hr in growth media. Cells were transfected with indicated empty vector, WT or C115S BDH1 plasmids using PolyJet transfection reagent (Signagen) per manufacturer's instructions. After 24hr, cells were treated with vehicle or 100µM Ethyl ester SNO-cysteine (ECNO), which was freshly prepared by mixing equal volumes of 2M sodium nitrite with 2M acidified ethyl ester cysteine (0.5M HCl) (Millipore-Sigma) to generate 1M ECNO, which was immediately added to designated cells at a final concentration of 100µM. Vehicle was prepared in the same manner, with omission of ethyl ester cysteine from 0.5M HCl. At the completion of the experiment, cells were harvested, pelleted, washed 1x with cold PBS, and subsequently resuspended in NP40 lysis buffer for biochemical analysis.

Cycloheximide pulse-chase assay

Cycloheximide pulse-chase assay (CHX chase) was performed using CHX (stock concentration: 10mg/mL in ddH_2O; Sigma Aldrich, cat#01810) added directly to cell culture media (at the time of ECNO/vehicle addition) to a final concentration of 100µg/mL for the indicated time period. At the end of the indicated time period, cells were harvested, washed 1x with cold PBS, and immediately frozen at -80°C. Once all timepoints were collected, all samples were thawed and immediately lysed in NP40 lysis buffer for biochemical analysis.

Cloning, expression and purification of recombinant SCoR2

The human SCoR2 coding sequence was previously cloned into the pET21b vector (*104*) to introduce a C-terminal 6xHis tag on the expressed protein. The recombinant SCoR2 protein was purified from BL21-CodonPlus Competent *E. coli* cells (Agilent). Overnight *E. coli* cultures were sub-cultured into 1 L of LB medium at 5%. At OD600 of 0.5, cultures were induced with 1 mM IPTG (Invitrogen) and grown for a further 4 hr at 28°C. Cultures were centrifuged at 4000g for 10 min to harvest the cells. Cell pellets from 1 L cultures were lysed in 10 mL of 1 x PBS buffer containing 1 mM PMSF (cat# P7626; Sigma), protease-inhibitor cocktail (Roche), DNAse 1 (cat# 260913; Sigma-Aldrich; final: 5µg/mL) and lysozyme (Sigma, cat#L6876; final: 1mg/mL) by sonication. Supernatant was clarified and SCoR2-His purified via HisTrap column (Cytiva; cat#17524801); binding with 20mM imidazole and elution with 500mM imidazole using Cytiva AKTA Pure chromatography system, followed by buffer exchange to assay buffer (50mM borate, 0.1mM EDTA, pH 9.0). Protein was concentrated using Ultra-15 centrifugal filters (Amicon), and concentration determined by BCA assay (Thermo Scientific; cat#23223/4). Purification was assessed by SDS-PAGE followed by Imperial Protein Stain (Thermo Fisher).

Mice

Mouse studies were approved by the Case Western Reserve University Institutional Animal Care and Use Committee (IACUC). Housing and procedures complied with the Guide for the Care and Use of Laboratory Animals and the American Veterinary Medical Association guidelines on euthanasia. SCoR2$^{+/-}$ mice were made by Deltagen, Inc. as described previously (*33*). The mice used in this manuscript were bred using SCoR2$^{-/-}$ male mice mated with SCoR2$^{+/-}$ female mice (SCoR2$^{-/-}$ female mice do not breed efficiently) to generate SCoR2$^{-/-}$ offspring which were used for the experiments described here. SCoR2$^{+/+}$ mice were generated from the offspring of SCoR2$^{+/-}$ male and female mice, and were occasionally backcrossed during the generation of the data in this manuscript. SCoR2$^{-/-}$ mice were fed with AIN-93M diet supplemented with 1% L-ascorbic acid (vitamin C) (Research Diets, Cat# D16021012, custom diet) to correct for the inability of AKR1A1/SCoR2$^{-/-}$ mice to synthesize L-ascorbic acid, as described previously (*36*). SCoR2$^{+/+}$ mice were fed with control AIN-93M diet (Research Diets, Cat# D10012M).

Myocardial ischemia/reperfusion (I/R) injury

Healthy male SCoR2$^{+/+}$ and SCoR2$^{-/-}$ mice (C57BL/6 background) aged 9-16 weeks were used for surgery. The female heart differs from the male heart in post-MI survival and cardiac function (*105–109*) and are more resilient following injury (*110*), making protection from tissue injury in female SCoR2$^{-/-}$ mice difficult to discern. Thus, distinct biology underlies the cardiac response to injury in female mice, and SCoR2$^{-/-}$-mediated cardioprotection in female mice is deserving of a separate study. Myocardial I/R injury was carried out as described previously (*111*). Briefly, mice were anesthetized, intubated and actively ventilated (respiration rate = ~133/min and tidal volume = ~200μL). The thoracic cavity was accessed through the left, third intercostal space and the

pericardium was resected to visualize the left anterior descending artery (LAD). A ligature of 7-0 silk suture was placed around the LAD and tightened to fully occlude arterial flow as verified by ischemic change in coloration of the anterior wall and by EKG tracings (ST-segment elevation). Following 30 min of ischemia, reperfusion was initiated by untying the suture. Following closure of the chest, pneumothorax was resolved by blunt needle aspiration. Mice were given 0.9% saline i.p. (0.5 mL/25g body weight) and were recovered under temperature support. Following 1-4hr reperfusion, mice for organ harvesting were anesthetized, whole blood harvested from IVC, spun and plasma collected, and LV, RV and lung tissue harvested and snap-frozen in liquid nitrogen for biochemical analysis. Mice harvested for tissue following 1hr reperfusion were excluded from survival analysis (Fig. 1G). Mice destined for infarct size evaluation following 24-hr reperfusion were anesthetized, the chest was opened, and a catheter was inserted into the transverse aorta. The right atrium was opened and 0.5 mL of 0.9% saline was administered through the aortic cannula to exsanguinate the heart. The LAD was then occluded with the in-dwelling suture and 0.2 mL of Evans blue (2% w/v) was injected into the LAD via the ascending aorta before the heart was extracted. The isolated heart was then frozen and sliced into segments 1 mm thick, and slices were placed in 1% TTC (2,3,5-triphenyltetrazolium chloride) in saline at 37°C for 20 min. TTC-stained slices were fixed in 10% formalin for 20 min before photographic documentation. Images were analyzed as described previously (*111*), with Image Pro Plus to evaluate area-at-risk (red), area of necrosis (white) and total LV area.

Echocardiography

Following 24-hr reperfusion, mice were anesthetized with 2,2,2-tribromoethanol (0.25 mg/g body weight, IP), and transthoracic echocardiography was performed using a Vevo 770 High-Resolution Imaging System equipped with an RMV-707B 30-MHz probe (VisualSonics). Standard M-mode

sampling was used through the left ventricular short axis at the midpapillary level. Ejection fraction, fractional shortening, LVID-s and other parameters were determined using the system's software.

Troponin-1 and LDH measurement

Mouse cardiac troponin-1 and LDH were measured using troponin-1 ELISA (cat#: KT-470; Kamiya) and LDH activity assay (cat#: MAK066-1KT; Sigma) kits, respectively, according to the manufacturer's instructions.

Terminal Uridine Deoxynucleotidyl Transferase dUTP Nick End Labeling (TUNEL Assay)

Heart tissue from SCoR2+/+ and SCoR2-/- mice post-MI were harvested, fixed in 4% paraformaldehyde overnight, switched to PBS and sectioned with 10 μm thickness onto microscope slides in preparation for TUNEL assay. Slides were baked at 60°C for 75 min, deparaffinized in 2 changes of xylene, rehydrated in graded ethanols (100%, 95%, 70%), and washed in PBS. Slides were pretreated with IHC Select Proteinase K (Chemicon International; cat# 21627) at final concentration of 20 μg/mL for 10 min at 25°C, then washed twice in dH_2O. Endogenous peroxidase activity was quenched with Peroxidazed 1 (BioCare Medical; cat# PX968G) for 8 min at 25°C, followed by 2x washes in dH_2O. Excess liquid removed and 900μL equilibration buffer (Chemicon Intl ApopTag Peroxidase In Situ Apoptosis Detection Kit; cat# S7100) applied for 10 sec at 25°C. Excess liquid tapped off, and TdT enzyme applied (ApopTag kit, 80% reaction buffer + 20% TdT enzyme) for 1 hr incubation at 37°C in a humidified chamber. TdT enzyme activity stopped with stop/wash buffer, agitated for 15 sec, incubated for 10 min at 25°C, and washed 3x in PBS. Anti-digoxigenin peroxidase conjugate (ApopTag kit) was applied and incubated for 30 min at 25°C in a humidified chamber, followed by 4 washes in PBS. 2 drops

DAB chromogen added to 2.0 mL DAB substrate to form Betazoid DAB (BioCare; cat# BDB2004L), and slides incubated in Betazoid DAB for 5 min in the dark at 25°C, followed by 3 washes in dH_2O and 5 min incubation in dH_2O. Slides then counterstained with CAT Hematoxylin (BioCare; cat# CATHE-M) for 30 sec, rinsed in dH_2O, dipped 10x in PBS, rinsed in tap water, air dried overnight, dipped in xylene for 10 sec, and coverslip applied with a resinous medium. Slides were imaged using brightfield 10x on a confocal microscope, $TUNEL^+$ nuclei quantified and analyzed by GraphPad Prism.

S-nitrosothiol Resin Assisted Capture (SNORAC)

SNORAC (*112*) was carried out as described previously (*33*). Mouse heart samples were mechanically homogenized in lysis buffer containing 100mM HEPES/1mM EDTA/100µM neocuproine (HEN), 50mM NaCl, 0.1% (vol/vol) Nonidet P-40, the thiol-blocking agent 0.2% S-methylmethanethiosulfonate (MMTS), 1mM PMSF and protease inhibitor (Roche). After centrifugation (10,000g, 4C, 20 min, x2), SDS and MMTS were added to the supernatant to 2.5% and 0.2% respectively, and incubated at 50C for 20 min. Proteins were precipitated with -20°C acetone, and redissolved in 1mL of HEN/1% SDS, repeated, and the final pellets were resuspended in HEN/1% SDS and protein concentrations determined using the Bicinchoninic Acid (BCA) method. Total lysates (typically 1-2 mg) were incubated with freshly prepared 50 mM ascorbate and 100 µl thiopropyl-Sepharose (50% slurry; made in-house as described previously (*113*)) and rotated end-over-end in the dark for 3 hr. The bound SNO-proteins were sequentially washed with HEN/1% SDS and 10% HEN/0.1% SDS; SNO-proteins were then eluted with 10% HEN/1% SDS/10% β-mercaptoethanol and analyzed by SDS/PAGE and immunoblotting with antibodies targeting proteins of interest.

Protein extraction and digestion (SCoR2 nitrosoproteome analysis)

For the SCoR2 nitrosoproteome analysis (SNORAC coupled to LC-MS/MS), SNO-proteins from heart lysates from N=4 mice for each condition were bound to thiopropyl-Sepharose beads, eluted using 2X Laemmli buffer with 10% β-mercaptoethanol, and provided to IQ Proteomics (Framingham, MA). Proteins were extracted by methanol-chloroform precipitation and digested with 0.5 ug of LysC for 12 hours at room temperature followed by 1 µg of trypsin (Promega) in 100 mM EPPS buffer (pH 8.0) for 4 hours at 37°C. A miscleavage rate check was performed on two random samples to ensure efficient digestion of proteins. Each of the eight tryptic peptide samples were labeled with 120 µg of Tandem Mass Tag (TMT10; Pierce) isobaric reagents for 2 hours at room temperature. A label efficiency check was performed by pooling 1 µL from each sample within a single plex to ensure at least 98% labeling of all N-termini and lysine residues. All samples were quenched with hydroxylamine (0.5%), acidified with trifluoroacetic acid (2%), pooled, and dried by vacuum centrifugation. Pooled TMT10 labeled peptides were reconstituted in 0.1%TFA and subjected to orthogonal basic-pH reverse phase fractionation on a 2.1 x 50mm column packed with 1.8um ZORBAX Extend-C18 material (Agilent) and equilibrated with buffer A (5% acetonitrile in 10mM ammonium bicarbonate, pH 8). Peptides were fractionated utilizing a 7min linear gradient from 5% to 50% buffer B (90% acetonitrile in 10mM ammonium bicarbonate, pH 8) at a flow rate of 0.3mL/min. A total of six fractions were collected and consolidated into 3 fractions and vacuum dried. The peptides were reconstituted in 0.2%FA and desalted with Empore-C18 (3M) in- house packed StageTips prior to analysis by mass spectrometry.

Mass spectrometry analysis and data search (SCoR2 nitrosoproteome analysis)

All mass spectra were acquired on an Orbitrap Fusion Lumos coupled to an EASY nanoLC-1200 (ThermoFisher) liquid chromatography system by IQ Proteomics (Framingham, MA).

Approximately 2 µg of peptides were loaded on a 75 µm capillary column packed in-house with Sepax GP-C18 resin (1.8 µm, 150 Å, Sepax) to a final length of 35 cm. Peptides were separated using a 120-minute linear gradient from 10% to 40% acetonitrile in 0.1% formic acid. The mass spectrometer was operated in a data dependent mode. The scan sequence began with FTMS1 spectra (resolution = 120,000; mass range of 350- 1400 m/z; max injection time of 50 ms; AGC target of 1e6; dynamic exclusion for 60 seconds with a +/- 10 ppm window). The 10 most intense precursors were selected within a 2 s cycle and fragmented via collisional-induced dissociation (CID) in the ion trap (normalized collision energy (NCE) = 35; max injection time = 35ms; isolation window of 0.7 Da; AGC target of 1e4). Following ITMS2 acquisition, a real-time search (RTS) algorithm was employed to score each peptide and only trigger synchronous-precursor-selection (SPS) MS3 quantitative spectra for high confidence scoring peptides as determined by a linear discriminant approach. Following MS2 acquisition, a synchronous-precursor-selection (SPS) MS3 method was enabled to select eight MS2 product ions for high energy collisional-induced dissociation (HCD) with analysis in the Orbitrap (NCE = 55 for TMT10; resolution = 50,000; max injection time = 86 ms; AGC target of 1.4e5; isolation window at 1.2 Da for +2 m/z, 1.0 Da for +3 m/z or 0.8 Da for +4 to +6 m/z). All mass spectra were converted to mzXML using a modified version of ReAdW.exe. MS/MS spectra were searched against a concatenated 2018 mouse Uniprot protein database containing common contaminants (forward + reverse sequences) using the SEQUEST algorithm (*114*). Database search criteria are as follows: fully tryptic with two missed cleavages; a precursor mass tolerance of 50 ppm and a fragment ion tolerance of 1 Da; oxidation of methionine (+15.9949 Da) was set as differential modifications. Static modifications were carboxyamidomethylation of cysteines (+57.0215 Da) and TMT on lysines and N-termini of peptides (modification mass for TMT10 is +229.1629 Da). Peptide-spectrum matches were filtered using linear discriminant analysis (*115*) and adjusted to a 1% peptide false discovery rate (FDR)

(*116*) and collapsed further to a final 1.0% protein-level FDR. Proteins were quantified by summing the total reporter intensities across all matching PSMs.

LC-MS/MS analysis and data search (SCoR2 interactome)

For the SCoR2 interactome analysis, hearts isolated from N=4 wild type mice were mechanically homogenized in non-denaturing lysis buffer (20mM Tris-HCl (pH 8.0), 137mM NaCl, 1% NP-40, 2mM EDTA), clarified, and incubated with 10ug of anti-SCoR2/AKR1A1 antibody (15054-1-AP, Proteintech) for 2 hours at room temperature. Sample was then incubated with 0.25mg pre-washed protein A/G magnetic beads (cat# 88802; Thermo Scientific) for 1 hour at room temperature while mixing and placed into a magnet for washing steps. Proteins were eluted from beads with 0.1M glycine (pH 2.0) for 10min at room temperature with agitation, magnetically separated, sample collected, neutralized with 15uL alkaline buffer (Tris, pH 8.0), and sent to the CWRU Proteomics and Small Molecule MS Core facility. Proteins were reduced with 10 mM dithiothreitol for 1 h at 37°C, followed by alkylation with 25 mM iodoacetamide for 30 min in the dark. After reduction/alkylation of proteins, dual digestion was performed with 0.3 µg of lysyl endopeptidase on a dry bath shaker for 1 h at 37°C followed by the addition of 0.3 µg of trypsin with incubation overnight at 37°C. After digestion, samples were filtered with 0.22 µM spin filters to remove any particulates before mass spectrometry (MS) analysis (Costar Spin-X; Sigma-Aldrich). Peptides were identified using data-dependent MS acquisition.

Samples were analyzed on an Orbitrap Eclipse mass spectrometer (Thermo Electron, San Jose, CA) equipped with a Waters nanoACQUITY LC system (Waters, Taunton, MA). Peptides were desalted in a trap column (180 µm × 20 mm, packed with C18 Symmetry, 5 µm, 100 Å; Waters) and subsequently resolved on a reversed-phase column (75 µm × 250 mm nanocolumn, packed with C18 BEH130, 1.7 µm, 130Å (Waters). Liquid chromatography was carried out at ambient

temperature at a flow rate of 300 nL/min using a gradient mixture of 0.1% formic acid in water (solvent A) and 0.1% formic acid in acetonitrile (solvent B). The gradient used ranged from 1% to 60% solvent B over 90 min. Nanospray was conducted in a positive ion mode with a voltage of 2.4 kV. A full scan was obtained for eluted peptides in the range of 375–1500 atomic mass units followed by 25 data-dependent MS/MS scans.

MS/MS spectra were generated by collision-induced dissociation of the peptide ions at normalized collision energy of 35% to generate a series of b- and y-ions as major fragments. A 1-hour wash step was performed between each sample.

LC-MS/MS results were analyzed in Mascot (version 2.7.0) (Matrix Science, London, United Kingdom). The database used was *Mus musculus* UniProt (17,089 proteins). Search settings were as follows: trypsin enzyme specificity; mass accuracy window for precursor ion, 10.0 ppm; mass accuracy window for fragment ions, 0.60 Da, and 1 missed cleavage. For the interactome experiment, carbamidomethyl of cysteine was specified in Mascot as a fixed modification and oxidation of methionine was specified in Mascot as a variable modification.

LC/MS-based untargeted metabolite profiling (metabolomic analysis)

Metabolite extraction and ratiometric profiling utilized acetonitrile (ACN), isopropanol (IPA), and methanol (MeOH) that were purchased from Fisher Scientific. High-purity Millipore filtered and deionized water (ddH2O; >18 MOhm) was used in extraction media and chromatography mobile phases. OmniTrace glacial acetic acid and ammonium hydroxide were obtained from EMD Chemicals. Ammonium acetate, ammonium formate, and all other chemicals and standards were obtained from Sigma-Aldrich in the best available grade.

Left ventricle was isolated from mice post-sham, 1hr I/R, or 4hr I/R, N=5 each condition and snap frozen in liquid nitrogen. Once received, tissue samples were washed with ice-cold PBS, followed

by metabolite extraction using −70°C 80:20 methanol:water (LC/MS grade methanol, Fisher Scientific). The tissue–methanol mixture was subjected to bead-beating for 45 s using a Tissuelyser cell disrupter (Qiagen). Extracts were centrifuged for 5 min at 18,500 x *g* to pellet insoluble protein and supernatants were transferred to clean tubes. The extraction procedure was repeated two additional times and all three supernatants were pooled, dried in a Vacufuge (Eppendorf), and stored at −80°C until analysis. The methanol-insoluble protein pellet was solubilized in 0.2 M NaOH at 95°C for 20 min and protein was quantified using a BioRad DC assay. On the day of metabolite analysis, dried cell extracts were reconstituted in 70% acetonitrile at a relative protein concentration of 4 µg/ml, and 4 µl of this reconstituted extract was injected for LC/MS-based targeted and untargeted metabolite profiling.

Tissue extracts were analyzed by LC/MS as described previously (*117*), using a platform comprised of an Agilent Model 1290 Infinity II liquid chromatography system coupled to an Agilent 6550 iFunnel time-of-flight MS analyzer. Chromatography of metabolites utilized aqueous normal phase (ANP) chromatography on a Diamond Hydride column (Microsolv, cat# 70000-15D-2, 4um, 2.1mm ID x 150mm Length, 100A). Mobile phases consisted of (A) 50% isopropanol, containing 0.025% acetic acid, and (B) 90% acetonitrile containing 5 mM ammonium acetate. To eliminate the interference by metal ions on chromatographic peak integrity and electrospray ionization, EDTA was added to the mobile phase at a final concentration of 5 µM. The following gradient was applied: 0–1.0 min, 99% B; 1.0–15.0 min, to 20% B; 15.0 to 29.0, 0% B; 29.1 to 37 min, 99% B. Raw data were analyzed using MassHunter Profinder 8.0 and MassProfiler Professional (MPP) 15.1 software (Agilent). Student's t-tests ($P < 0.05$) were performed to identify significant differences between groups.

Peripheral blood was isolated fresh from murine IV post-sham, 1hr I/R, or 4hr I/R, N=5 each condition, into BD microtainer (cat#365967; BD) tubes for blood separation after 30 min room-

temperature incubation followed by centrifugation at 1500 g for 5 min. Plasma was then snap-frozen and sent for LC/MS analysis. Plasma metabolites were extracted by the addition of 1 part plasma to 20 parts 70% acetonitrile in ddH_2O (vol:vol). The mixture was briefly vortexed and then centrifuged for 5 min at 16,000 *g* to pellet precipitated proteins. An aliquot of the resulting extract (3 µl) was subjected to LC/MS-based untargeted metabolite profiling in both positive and negative ion modes.

Metabolite structure specification

To ascertain the identities of differentially expressed metabolites ($P < 0.05$), LC/MS data were searched against an in-house annotated personal metabolite database created using MassHunter PCDL manager 8.0 (Agilent), based on monoisotopic neutral masses (< 5 ppm mass accuracy) and chromatographic retention times. A molecular formula generator (MFG) algorithm in MPP was used to generate and score empirical molecular formulae, based on a weighted consideration of monoisotopic mass accuracy, isotope abundance ratios, and spacing between isotope peaks. A tentative compound ID was assigned when PCDL database and MFG scores concurred for a given candidate molecule. Tentatively assigned molecules were verified based on a match of LC retention times and/or MS/MS fragmentation spectra for pure molecule standards contained in a growing in-house metabolite database.

Bioinformatics

All studies were done in at least triplicate, unless otherwise noted. Studies using mice utilized at least 3 mice per condition/treatment. All metabolomic studies used 5 mice per group. Co-IP mass spectrometry data (CWRU) were obtained as unique spectrum count, and SNORAC mass spectrometry data (IQ Proteomics) were obtained as normalized summed signal/noise values for

each identified protein. In the interactome study, proteins with an average of ≥ 1 unique spectrum count across 3 mouse heart samples were identified as interacting proteins and included in the 'interactome' list. In the SNORAC/MS nitrosoproteome study, all SNO-proteins identified in SCoR2$^{-/-}$ mouse heart with values ≥ 1.2-fold change relative to those identified in SCoR2$^{+/+}$ mouse heart, in at least 2 out of 4 experimental sets, were included in the final "SNO-ome" list.

Western blot analysis

Proteins were extracted from cells or tissues and subjected to 4-20% Criterion Precast Midi Protein Gel electrophoresis. Blotted membranes were incubated overnight at 4°C with primary antibodies, washed with PBS+0.1% Tween-20, then incubated with HRP-conjugated secondary antibody (anti-mouse or anti-rabbit IgG (Promega)) for 1hr followed by chemiluminescent detection (ECL (GE Healthcare)). Antibodies employed in Western blotting included: rabbit polyclonal anti-AKR1A1/SCoR2 (15054-1-AP, Proteintech Group), rabbit monoclonal anti-PKM2 (D78A4, Cell Signaling), mouse monoclonal anti-p97 (10R-P104A, Fitzgerald), rabbit polyclonal anti-BDH1 (15417-1-AP, Proteintech Group). Coomassie blots used Imperial Protein Stain (cat#24615; Thermo Scientific) with 1hr staining followed by 3 hours washing. Quantification of Western blots was carried out with ImageJ (NIH).

Assay of NADPH-dependent SCoR2 activity with SNO-CoA or carbohydrates as substrate

The NADPH-dependent SNO-CoA reductase activity of recombinant SCoR2 was determined spectrophotometrically as described previously (*104*). Briefly, the assays were performed in 50mM phosphate buffer (pH 7.0; containing 0.1mM EDTA and DTPA) with 186nM SCoR2, 100µM NADPH and substrate: 100µM SNO-CoA as positive control or 1mM of specific test carbohydrates (L-(+)-arabinose, D-(-)-ribose, D-(-)-erythrose, D-(+)-glucose, D-(-)-fructose, D-

(+)-galactose, sucrose, D-ribulose, D-xylulose). Reactions were initiated by the addition of recombinant SCoR2 and allowed to proceed for 1 min while NADPH consumption was measured by spectrophotometer.

NADPH-Glo assay

NADPH/$NADP^+$ assay was performed with NADP/NADPH-Glo Assay kit (Promega), as per the manufacturer's instructions. Mouse heart samples (2 µg/mL) were mechanically homogenized in EBC lysis buffer containing protease inhibitor cocktail (Roche), clarified, plated in triplicate, and manufacturer's protocol followed. Luminescence was recorded using Promega GloMax Discover instrument.

cGMP measurement

cGMP ELISA was performed using Cyclic GMP Complete kit (Enzo; cat#ADI-900-164) as per the manufacturer's instructions. Mouse heart samples (post-I/R with 1 hr reperfusion) were homogenized in 10 volumes of 0.1M HCl, centrifuged at 600g for 10 min, and supernatant diluted 1:20 and run directly in the assay. Assay results in pmol cGMP/mL were normalized between samples by dividing by protein concentration as determined by BCA assay, and results displayed as pmol cGMP/mg total protein.

Human subjects

De-identified human post-mortem myocardial specimens with basic clinical data (sample type, sex, age, race) were collected by the Duke Human Heart Repository (Duke University IRB# Pro00005621) and obtained in the de-identified state. Experiments at CWRU involving these samples (study#: STUDY20230090) were determined by the CWRU IRB to be categorized as

research not involving human subjects and therefore not requiring separate CWRU IRB review and approval.

Mouse subjects

All experimental procedures were approved by the Institutional Animal Care and Use Committee of Case Western Reserve University School of Medicine and were conducted in accordance with the NIH *Guide for the Care and Use of Laboratory Animals* (National Academies Press. 2011). All potentially painful procedures were conducted under a surgical plane of anesthesia (typically ketamine/xylazine 100/10 mg/kg), and mice were sacrificed by methods compliant with the American Veterinary Medical Association (AMVA) *Guidelines for Euthanasia of Animals* (2013 edition).

Statistical Analysis

Data are presented as mean ± SD except where noted, with median and range reported in supplementary materials (Table S3). Parametric and non-parametric tests of statistical significance, as appropriate and indicated within each figure legend, were used to test for strain and treatment effects. Parametric tests were used if normality was satisfied, and non-parametric tests were used if normality was not satisfied or could not be confirmed due to $n < 5$ independent replicates. Analysis was performed using GraphPad Prism software (v9). Under all conditions, P values < 0.05 were taken to indicate a statistically significant difference between groups.

Acknowledgments:

The authors acknowledge the assistance of Kathleen Lundberg at the Proteomics and Small Molecule Mass Spectrometry Core and of Adam Kresak and Jennifer Mikulan at the Tissue

Resource Core at Case Western Reserve University, Isobel Taylor for assisting with metabolomics data acquisition at Weill Cornell Graduate School of Medical Sciences, the staff at the Human Heart Repository at Duke University, and the IQ Proteomics team in Framingham, MA.

Funding:

This work was supported in part by:

National Institutes of Health grant P01HL158507 (JSS)

National Institutes of Health grant R01HL126900 (JSS)

National Institutes of Health grant RO1DK119506 (JSS)

National Institutes of Health grant RO1DK128347 (JSS)

American Heart Association-Allen grant 19PABH134580006 (JSS)

National Institutes of Health grant R01HL157151 (WJK and JSS)

National Institutes of Health grant RO1AR076029 (QC)

National Institutes of Health grant RO1NS131322 (SSG)

National Institutes of Health MSTP grant 2T32GM007250-44 (ZWG)

Author contributions:

Conceptualization, Z.W.G, and J.S.S.; Methodology, Z.W.G, H.L.Z, Q.C., D.M.; Formal Analysis, Z.W.G, R.Z., Q.C., D.M.; Investigation, Z.W.G., R.Z., H.L.Z., Q.C, D.M., J.L. R.K.; Writing – Original Draft, Z.W.G.; Writing – Review and Editing, Z.W.G., R.T.P., W.J.K., S.S.G., and J.S.S.; Supervision, W.J.K., S.S.G., and J.S.S.; Funding Acquisition, J.S.S.

Competing interests:

Jonathan Stamler is a founder and board member of and has equity interest in SNO bio, a company developing nitrosylation related therapeutics, and NNOXX, a company developing NO-based

device technology. CWRU and UHCMC are aware of these conflicts and appropriate management plans are in place. None of the other authors have relevant conflicts to disclose.

Data and materials availability:

All data are available in the main text or in the supplementary materials.

REFERENCES

1. Tsao, C. W., Aday, A. W., Almarzooq, Z. I., Anderson, C. A. M., Arora, P., Avery, C. L., Baker-Smith, C. M., Beaton, A. Z., Boehme, A. K., Buxton, A. E., Commodore-Mensah, Y., Elkind, M. S. V., Evenson, K. R., Eze-Nliam, C., Fugar, S., Generoso, G., Heard, D. G., Hiremath, S., Ho, J. E., Kalani, R., Kazi, D. S., Ko, D., Levine, D. A., Liu, J., Ma, J., Magnani, J. W., Michos, E. D., Mussolino, M. E., Navaneethan, S. D., Parikh, N. I., Poudel, R., Rezk-Hanna, M., Roth, G. A., Shah, N. S., St-Onge, M. P., Thacker, E. L., Virani, S. S., Voeks, J. H., Wang, N. Y., Wong, N. D., Wong, S. S., Yaffe, K. & Martin, S. S. *Heart Disease and Stroke Statistics - 2023 Update: A Report from the American Heart Association*. *Circulation* **147,** (2023).
2. Stone, G. W., Selker, H. P., Thiele, H., Patel, M. R., Udelson, J. E., Ohman, E. M., Maehara, A., Eitel, I., Granger, C. B., Jenkins, P. L., Nichols, M. & Ben-Yehuda, O. Relationship between Infarct Size and Outcomes Following Primary PCI Patient-Level Analysis from 10 Randomized Trials. *J Am Coll Cardiol* **67,** 1674–1683 (2016).
3. Johansson, S., Rosengren, A., Young, K. & Jennings, E. Mortality and morbidity trends after the first year in survivors of acute myocardial infarction: A systematic review. *BMC Cardiovasc Disord* **17,** 1–8 (2017).
4. Hausenloy, D. J. & Yellon, D. M. Myocardial ischemia-reperfusion injury: A neglected therapeutic target. *Journal of Clinical Investigation* **123,** 92–100 (2013).
5. Heusch, G. Critical Issues for the Translation of Cardioprotection. *Circ Res* **120,** 1477–1486 (2017).
6. Lefer, D. J. & Marbán, E. Is Cardioprotection Dead? *Circulation* **136,** 98–109 (2017).
7. Bolli, R. Cardioprotective Function of Inducible Nitric Oxide Synthase and Role of Nitric Oxide in Myocardial Ischemia and Preconditioning: An Overview of a Decade of Research. *J Mol Cell Cardiol* **33,** 1897–1918 (2001).
8. Schulz, R., Kelm, M. & Heusch, G. Nitric oxide in myocardial ischemia/reperfusion injury. *Cardiovasc Res* **61,** 402–413 (2004).
9. Janssens, S., Pokreisz, P., Schoonjans, L., Pellens, M., Vermeersch, P., Tjwa, M., Jans, P., Scherrer-Crosbie, M., Picard, M. H., Szelid, Z., Gillijns, H., Van De Werf, F., Collen, D. & Bloch, K. D. Cardiomyocyte-specific overexpression of nitric oxide synthase 3 improves left ventricular performance and reduces compensatory hypertrophy after myocardial infarction. *Circ Res* **94,** 1256–1262 (2004).
10. Lima, B., Lam, G. K. W., Xie, L., Diesen, D. L., Villamizar, N., Nienaber, J., Messina, E., Bowles, D., Kontos, C. D., Hare, J. M., Stamler, J. S. & Rockman, H. A. Endogenous S-nitrosothiols protect against myocardial injury. *Proc Natl Acad Sci U S A* **106,** 6297–6302 (2009).
11. Gonzalez, F. M., Shiva, S., Vincent, P. S., Ringwood, L. A., Hsu, L.-Y., Hon, Y. Y., Aletras, A. H., Cannon III, R. O., Gladwin, M. T. & Arai, A. E. Nitrite Anion (NO2 −) Provides Potent Cytoprotective and Anti- apoptotic Effects as Adjunctive Therapy to Reperfusion for Acute Myocardial Infarction. *Circulation* **117,** 2986–2994 (2008).
12. Dezfulian, C., Shiva, S., Alekseyenko, A., Pendyal, A., Beiser, D. G., Munasinghe, J. P., Anderson, S. A., Chesley, C. F., Vanden Hoek, T. L. & Gladwin, M. T. Nitrite therapy after cardiac arrest reduces reactive oxygen species generation, improves cardiac and neurological function, and enhances survival via reversible inhibition of mitochondrial complex I. *Circulation* **120,** 897–905 (2009).

13. Duranski, M. R., Greer, J. J. M., Dejam, A., Jaganmohan, S., Hogg, N., Langston, W., Patel, R. P., Yet, S. F., Wang, X., Kevil, C. G., Gladwin, M. T. & Lefer, D. J. Cytoprotective effects of nitrite during in vivo ischemia-reperfusion of the heart and liver. *Journal of Clinical Investigation* **115,** 1232–1240 (2005).
14. Sun, J., Morgan, M., Shen, R. F., Steenbergen, C. & Murphy, E. Preconditioning results in S-nitrosylation of proteins involved in regulation of mitochondrial energetics and calcium transport. *Circ Res* **101,** 1155–1163 (2007).
15. Seth, D., Hess, D. T., Hausladen, A., Wang, L., Wang, Y. & Stamler, J. S. A Multiplex Enzymatic Machinery for Cellular Protein S- nitrosylation. *Mol Cell* **69,** 451–464 (2018).
16. Zhou, H.-L., Grimmett, Z. W., Venetos, N. M., Stomberski, C. T., Qian, Z., McLaughlin, P. J., Bansal, P. K., Zhang, R., Reynolds, J. D., Premont, R. T. & Stamler, J. S. An enzyme that selectively S-nitrosylates proteins to regulate insulin signaling. *Cell* **186,** 5812-5825.e21 (2023).
17. Stomberski, C. T., Venetos, N. M., Zhou, H. L., Qian, Z., Collison, B. R., Field, S. J., Premont, R. T. & Stamler, J. S. A multienzyme S-nitrosylation cascade regulates cholesterol homeostasis. *Cell Rep* **41,** 111538 (2022).
18. Hayashida, K., Bagchi, A., Miyazaki, Y., Seth, D., Silverman, M. G., Rezoagli, E., Marutani, E., Mori, N., Magliocca, A., Liu, X., Berra, L., Hindle, A. G., Donnino, M. W., Malhotra, R., Bradley, M. O., Stamler, J. S., Ichinose, F., Hospital, M. G., Western, C., Hospital, M. G., Deaconess, B. I. & Western, C. Improvement in Outcomes After Cardiac Arrest and Resuscitation by Inhibition of S-Nitrosoglutathione Reductase. *Circulation* **139,** 815–827 (2019).
19. Tang, X., Zhao, S., Liu, J., Liu, X., Sha, X., Huang, C., Hu, L., Sun, S., Gao, Y., Chen, H., Zhang, Z., Wang, D., Gu, Y., Chen, S., Wang, L., Gu, A., Chen, F., Pu, J., Chen, X., Yu, B., Xie, L., Huang, Z., Han, Y. & Ji, Y. Mitochondrial GSNOR Alleviates Cardiac Dysfunction via ANT1 Denitrosylation. *Circ Res* 220–236 (2023). doi:10.1161/circresaha.123.322654
20. Whalen, E. J., Foster, M. W., Matsumoto, A., Ozawa, K., Violin, J. D., Que, L. G., Nelson, C. D., Benhar, M., Keys, J. R., Rockman, H. A., Koch, W. J., Daaka, Y., Lefkowitz, R. J. & Stamler, J. S. Regulation of β-Adrenergic Receptor Signaling by S-Nitrosylation of G-Protein-Coupled Receptor Kinase 2. *Cell* **129,** 511–522 (2007).
21. Huang, Z. M., Gao, E., Fonseca, F., Hayashi, H., Shang, X., Lefer, D. J., Stamler, J. S. & Koch, W. J. Convergence of G Protein-Coupled Receptor and Nitric Oxide Pathways Determines the Outcome to Cardiac Ischemic Injury. *Sci Signal* (2014). doi:10.1126/scisignal.2004225.3.
22. Anand, P., Hausladen, A., Wang, Y. J., Zhang, G. F., Stomberski, C., Brunengraber, H., Hess, D. T. & Stamler, J. S. Identification of S-nitroso-CoA reductases that regulate protein S-nitrosylation. *Proc Natl Acad Sci U S A* **111,** 18572–18577 (2014).
23. Stomberski, C. T., Zhou, H. L., Wang, L., Van Den Akker, F. & Stamler, J. S. Molecular recognition of S-nitrosothiol substrate by its cognate protein denitrosylase. *Journal of Biological Chemistry* **294,** 1568–1578 (2019).
24. Zhou, H.-L., Zhang, R., Anand, P., Stomberski, C. T., Qian, Z., Hausladen, A., Wang, L., Rhee, E. P., Parikh, S. M., Karumanchi, S. A. & Stamler, J. S. Metabolic reprogramming by the S-nitroso-CoA Reductase system protects from kidney injury. *Nature* **565,** 96–100 (2019).
25. Zhou, H. L., Hausladen, A., Anand, P., Rajavel, M., Stomberski, C. T., Zhang, R., Premont, R. T., Greenlee, W. J., van den Akker, F. & Stamler, J. S. Identification of a

Selective SCoR2 Inhibitor That Protects Against Acute Kidney Injury. *J Med Chem* **66,** 5657–5668 (2023).
26. Stomberski, C. T., Venetos, N. M., Zhou, H. L., Qian, Z., Collison, B. R., Field, S. J., Premont, R. T. & Stamler, J. S. A multienzyme S-nitrosylation cascade regulates cholesterol homeostasis. *Cell Rep* **41,** 111538 (2022).
27. Watanabe, K. GWAS Atlas PheWAS. at <https://atlas.ctglab.nl/PheWAS>
28. Watanabe, K., Stringer, S., Frei, O., Umićević Mirkov, M., de Leeuw, C., Polderman, T. J. C., van der Sluis, S., Andreassen, O. A., Neale, B. M. & Posthuma, D. A global overview of pleiotropy and genetic architecture in complex traits. *Nat Genet* **51,** 1339–1348 (2019).
29. Aragam, K. G., Chaffin, M., Levinson, R. T., McDermott, G., Choi, S. H., Shoemaker, M. B., Haas, M. E., Weng, L.-C., Lindsay, M. E., Smith, J. G., Newton-Cheh, C., Roden, D. M., London, B., Wells, Q. S., Ellinor, P. T., Kathiresan, S. & Lubitz, S. A. Phenotypic Refinement of Heart Failure in a National Biobank Facilitates Genetic Discovery. *Circulation* **139,** 489–501 (2019).
30. Cardiovascular Disease Knowledge Portal (broadcvdi.org). at <https://cvd.hugeamp.org/gene.html?gene=AKR1A1 (RRID:SCR_016536)>
31. Costanzo, M. C., Roselli, C., Brandes, M., Duby, M., Hoang, Q., Jang, D., Koesterer, R., Kudtarkar, P., Moriondo, A., Nguyen, T., Ruebenacker, O., Smadbeck, P., Sun, Y., Butterworth, A. S., Aragam, K. G., Lumbers, R. T., Khera, A. V, Lubitz, S. A., Ellinor, P. T., Gaulton, K. J., Flannick, J. & Burtt, N. P. Cardiovascular Disease Knowledge Portal: A Community Resource for Cardiovascular Disease Research. *Circ Genom Precis Med* **16,** e004181 (2023).
32. Kukreja, R. C., Salloum, F. N. & Das, A. Role of cGMP Signaling and Phosphodiesterase-5 inhibitors in Cardioprotection. *J Am Coll Cardiol* **59,** 1921–1927 (2012).
33. Zhou, H.-L., Zhang, R., Anand, P., Stomberski, C. T., Qian, Z., Hausladen, A., Wang, L., Rhee, E. P., Parikh, S. M., Karumanchi, S. A. & Stamler, J. S. Metabolic reprogramming by the S-nitroso-CoA Reductase system protects from kidney injury. *Nature* **565,** 96–100 (2019).
34. Stomberski, C. T., Venetos, N. M., Zhou, H. L., Qian, Z., Collison, B. R., Field, S. J., Premont, R. T. & Stamler, J. S. A multienzyme S-nitrosylation cascade regulates cholesterol homeostasis. *Cell Rep* **41,** 111538 (2022).
35. Zhou, H.-L., Grimmett, Z. W., Venetos, N. M., Stomberski, C. T., Qian, Z., McLaughlin, P. J., Bansal, P. K., Zhang, R., Reynolds, J. D., Premont, R. T. & Stamler, J. S. An enzyme that selectively S-nitrosylates proteins to regulate insulin signaling. *Cell* **186,** 5812-5825.e21 (2023).
36. Lai, C. W., Chen, H. L., Tu, M. Y., Lin, W. Y., Röhrig, T., Yang, S. H., Lan, Y. W., Chong, K. Y. & Chen, C. M. A novel osteoporosis model with ascorbic acid deficiency in Akr1A1 gene knockout mice. *Oncotarget* **8,** 7357–7369 (2017).
37. Lau, B., Fazelinia, H., Mohanty, I., Raimo, S., Tenopoulou, M., Doulias, P.-T. & Ischiropoulos, H. Endogenous S-nitrosocysteine proteomic inventories identify a core of proteins in heart metabolic pathways. *Redox Biol* **47,** 102153 (2021).
38. Aubert, G., Martin, O. J., Horton, J. L., Lai, L., Vega, R. B., Leone, T. C., Koves, T., Gardell, S. J., Krüger, M., Hoppel, C. L., Lewandowski, E. D., Crawford, P. A., Muoio, D. M. & Kelly, D. P. The Failing Heart Relies on Ketone Bodies as a Fuel. *Circulation* **133,** 698–705 (2016).
39. Nielsen, R., Møller, N., Gormsen, L. C., Tolbod, L. P., Hansson, N. H., Sorensen, J., Harms, H. J., Frøkiær, J., Eiskjaer, H., Jespersen, N. R., Mellemkjaer, S., Lassen, T. R.,

Pryds, K., Bøtker, H. E. & Wiggers, H. Cardiovascular Effects of Treatment With the Ketone Body 3-Hydroxybutyrate in Chronic Heart Failure Patients. *Circulation* **139,** 2129–2141 (2019).

40. Uchihashi, M., Hoshino, A., Okawa, Y., Ariyoshi, M., Kaimoto, S., Tateishi, S., Ono, K., Yamanaka, R., Hato, D., Fushimura, Y., Honda, S., Fukai, K., Higuchi, Y., Ogata, T., Iwai-Kanai, E. & Matoba, S. Cardiac-Specific Bdh1 Overexpression Ameliorates Oxidative Stress and Cardiac Remodeling in Pressure Overload-Induced Heart Failure. *Circ Heart Fail* **10,** 1–11 (2017).
41. Lau, B., Fazelinia, H., Mohanty, I., Raimo, S., Tenopoulou, M., Doulias, P.-T. & Ischiropoulos, H. Endogenous S-nitrosocysteine proteomic inventories identify a core of proteins in heart metabolic pathways. *Redox Biol* **47,** 102153 (2021).
42. Landoni, G., Zangrillo, A., Lomivorotov, V. V., Likhvantsev, V., Ma, J., De Simone, F. & Fominskiy, E. Cardiac protection with phosphocreatine: A meta-analysis. *Interact Cardiovasc Thorac Surg* **23,** 637–646 (2016).
43. Siragusa, M., Thöle, J., Bibli, S., Luck, B., Loot, A. E., Silva, K., Wittig, I., Heidler, J., Stingl, H., Randriamboavonjy, V., Kohlstedt, K., Brüne, B., Weigert, A., Fisslthaler, B. & Fleming, I. Nitric oxide maintains endothelial redox homeostasis through PKM2 inhibition. *EMBO J* **38,** 1–13 (2019).
44. Lazzeri, C., Valente, S., Chiostri, M. & Gensini, G. F. Clinical significance of lactate in acute cardiac patients. *World J Cardiol* **7,** 483–489 (2015).
45. Witkowski, M., Nemet, I., Alamri, H., Wilcox, J., Gupta, N., Nimer, N., Haghikia, A., Li, X., Wu, Y., Prasad Saha, P., Demuth, I., König, M., Steinhagen-Thiessen, E., Cajka, T., Fiehn, O., Landmesser, U., Tang, W. & Hazen, S. The Artificial Sweetener Erythritol and Cardiovascular Event Risk. *Nat Med* (2022). doi:10.1038/s41591-023-02223-9
46. Witkowski, M., Nemet, I., Li, X. S., Wilcox, J., Ferrell, M., Alamri, H., Gupta, N., Wang, Z., Tang, W. H. W. & Hazen, S. L. Xylitol is prothrombotic and associated with cardiovascular risk. *Eur Heart J* (2024). doi:10.1093/eurheartj/ehae244
47. Wamelink, M. M. C. & Williams, M. in *Physician's Guide to the Diagnosis, Treatment, and Follow-Up of Inherited Metabolic Diseases* (eds. Blau, N., Dionisi Vici, C., Ferreira, C. R., Vianey-Saban, C. & van Karnebeek, C. D. M.) 701–712 (Springer International Publishing, 2022). doi:10.1007/978-3-030-67727-5_40
48. Huck, J. H. J., Verhoeven, N. M., Struys, E. A., Salomons, G. S., Jakobs, C. & Van Der Knaap, M. S. Ribose-5-Phosphate Isomerase Deficiency: New Inborn Error in the Pentose Phosphate Pathway Associated with a Slowly Progressive Leukoencephalopathy. *Am J Hum Genet* **74,** 745–751 (2004).
49. Hamada, Y., Kitoh, R. & Raskin, P. Crucial role of aldose reductase activity and plasma glucose level in sorbitol accumulation in erythrocytes from diabetic patients. *Diabetes* **40,** 1233–1240 (1991).
50. Fujii, J., Homma, T., Miyata, S. & Takahashi, M. Pleiotropic actions of aldehyde reductase (Akr1a). *Metabolites* **11,** (2021).
51. Danesh, F. R., Wada, J., Wallner, E. I., Sahai, A., Srivastava, S. K. & Kanwar, Y. S. Gene regulation of aldose-, aldehyde- and a renal specific oxido reductase (RSOR) in the pathobiology of diabetes mellitus. *Curr Med Chem* **10,** 1399–1406 (2003).
52. Hicks, K. G., Cluntun, A. A., Schubert, H. L., Hackett, S. R., Berg, J. A., Leonard, P. G., Ajalla Aleixo, M. A., Zhou, Y., Bott, A. J., Salvatore, S. R., Chang, F., Blevins, A., Barta, P., Tilley, S., Leifer, A., Guzman, A., Arok, A., Fogarty, S., Winter, J. M., Ahn, H. C., Allen, K. N., Block, S., Cardoso, I. A., Ding, J., Dreveny, I., Gasper, W. C., Ho, Q.,

Matsuura, A., Palladino, M. J., Prajapati, S., Sun, P., Tittmann, K., Tolan, D. R., Unterlass, J., VanDemark, A. P., Vander Heiden, M. G., Webb, B. A., Yun, C. H., Zhao, P., Wang, B., Schopfer, F. J., Hill, C. P., Nonato, M. C., Muller, F. L., Cox, J. E. & Rutter, J. Protein-metabolite interactomics of carbohydrate metabolism reveal regulation of lactate dehydrogenase. *Science (1979)* **379,** 996–1003 (2023).

53. Mnatsakanyan, R., Markoutsa, S., Walbrunn, K., Roos, A., Verhelst, S. H. L. & Zahedi, R. P. Proteome-wide detection of S-nitrosylation targets and motifs using bioorthogonal cleavable-linker-based enrichment and switch technique. *Nat Commun* **10,** 1–12 (2019).
54. Hendgen-Cotta, U. B., Merx, M. W., Shiva, S., Schmitz, J., Becher, S., Klare, J. P., Steinhoff, H. J., Goedecke, A., Schrader, J., Gladwin, M. T., Kelm, M. & Rassaf, T. Nitrite reductase activity of myoglobin regulates respiration and cellular viability in myocardial ischemia-reperfusion injury. *Proc Natl Acad Sci U S A* **105,** 12636 (2008).
55. Siddiqi, N., Neil, C., Bruce, M., MacLennan, G., Cotton, S., Papadopoulou, S., Feelisch, M., Bunce, N., Lim, P. O., Hildick-Smith, D., Horowitz, J., Madhani, M., Boon, N., Dawson, D., Kaski, J. C. & Frenneaux, M. Intravenous sodium nitrite in acute ST-elevation myocardial infarction: A randomized controlled trial (NIAMI). *Eur Heart J* **35,** 1255–1262 (2014).
56. Jones, D. A., Pellaton, C., Velmurugan, S., Rathod, K. S., Andiapen, M., Antoniou, S., Van Eijl, S., Webb, A. J., Westwood, M. A., Parmar, M. K., Mathur, A. & Ahluwalia, A. Randomized phase 2 trial of intracoronary nitrite during acute myocardial infarction. *Circ Res* **116,** 437–447 (2015).
57. Horton, J. L., Davidson, M. T., Kurishima, C., Vega, R. B., Powers, J. C., Matsuura, T. R., Petucci, C., Lewandowski, E. D., Crawford, P. A., Muoio, D. M., Recchia, F. A. & Kelly, D. P. The failing heart utilizes 3-hydroxybutyrate as a metabolic stress defense. *JCI Insight* **4,** 1–19 (2019).
58. Mitchell, G. A., Kassovska-Bratinova, S., Boukaftane, Y., Robert, M. F., Wang, S. P., Ashmarina, L., Lambert, M., Lapierre, P. & Potier, E. Medical aspects of ketone body metabolism. *Clin Invest Med* **18,** 193–216 (1995).
59. Homilius, C., Seefeldt, J. M., Axelsen, J. S., Pedersen, T. M., Sørensen, T. M., Nielsen, R., Wiggers, H., Hansen, J., Matchkov, V. V, Bøtker, H. E. & Boedtkjer, E. Ketone body 3-hydroxybutyrate elevates cardiac output through peripheral vasorelaxation and enhanced cardiac contractility. *Basic Res Cardiol* **118,** 37 (2023).
60. Cotter, D. G., Schugar, R. C. & Crawford, P. A. Ketone body metabolism and cardiovascular disease. *Am J Physiol Heart Circ Physiol* **304,** H1060-76 (2013).
61. Zuurbier, C. J., Bertrand, L., Beauloye, C. R., Andreadou, I., Ruiz-Meana, M., Jespersen, N. R., Kula-Alwar, D., Prag, H. A., Eric Botker, H., Dambrova, M., Montessuit, C., Kaambre, T., Liepinsh, E., Brookes, P. S. & Krieg, T. Cardiac metabolism as a driver and therapeutic target of myocardial infarction. *J Cell Mol Med* **24,** 5937–5954 (2020).
62. Marina Prendes, M. G., García, J. V, Fernández, M. A., Pérez, M. J., Perazzo, J. C., Savino, E. A. & Varela, A. Effects of 5-hydroxydecanoate and ischemic preconditioning on the ischemic-reperfused heart of fed and fasted rats. *J Physiol Biochem* **61,** 447–456 (2005).
63. Snorek, M., Hodyc, D., Sedivý, V., Durišová, J., Skoumalová, A., Wilhelm, J., Neckář, J., Kolář, F. & Herget, J. Short-term fasting reduces the extent of myocardial infarction and incidence of reperfusion arrhythmias in rats. *Physiol Res* **61,** 567–574 (2012).
64. Hron, W., Menahan, L. & Lech, J. Inhibition of Hormonal Stimulation of Lipolysis in Perfused Rat Heart by Ketone Bodies. *J Mol Cell Cardiol* **10,** 161–174 (1978).

65. Zou, Z., Sasaguri, S., Rajesh, K. G. & Suzuki, R. Dl-3-Hydroxybutyrate Administration Prevents Myocardial Damage After Coronary Occlusion in Rat Hearts. *Am J Physiol Heart Circ Physiol* **283,** 1968–1974 (2002).
66. Yu, Y., Yu, Y., Zhang, Y., Zhang, Z., An, W. & Zhao, X. Treatment with D-β-hydroxybutyrate protects heart from ischemia/reperfusion injury in mice. *Eur J Pharmacol* **829,** 121–128 (2018).
67. Berg-Hansen, K., Christensen, K. H., Gopalasingam, N., Nielsen, R., Eiskjær, H., Møller, N., Birkelund, T., Christensen, S. & Wiggers, H. Beneficial Effects of Ketone Ester in Patients With Cardiogenic Shock. *JACC Heart Fail* (2023). doi:10.1016/j.jchf.2023.05.029
68. Lommi, J., Kupari, M., Koskinen, P., Näveri, H., Leinonen, H., Pulkki, K. & Härkönen, M. Blood ketone bodies in congestive heart failure. *J Am Coll Cardiol* **28,** 665–672 (1996).
69. Selvaraj, S., Kelly, D. P. & Margulies, K. B. Implications of Altered Ketone Metabolism and Therapeutic Ketosis in Heart Failure. *Circulation* **141,** 1800–1812 (2020).
70. Sato, J., Kinoshita, K. & Sakurai, A. Elevated blood acetoacetate levels reduce major adverse cardiac and cerebrovascular events risk in acute myocardial infarction. *Open Med (Wars)* **18,** 20230793 (2023).
71. Homilius, C., Seefeldt, J. M., Axelsen, J. S., Pedersen, T. M., Sørensen, T. M., Nielsen, R., Wiggers, H., Hansen, J., Matchkov, V. V, Bøtker, H. E. & Boedtkjer, E. Ketone body 3-hydroxybutyrate elevates cardiac output through peripheral vasorelaxation and enhanced cardiac contractility. *Basic Res Cardiol* **118,** 37 (2023).
72. Sharov, V. G., Afonskaya, N. I., Ruda, M. Y., Cherpachenko, N. M., Pozin, E. Y., Markosyan, R. A., Shepeleva, I. I., Samarenko, M. B. & Saks, V. A. Protection of ischemic myocardium by exogenous phosphocreatine (Neoton): Pharmacokinetics of phosphocreatine, reduction of infarct size, stabilization of sarcolemma of ischemic cardiomyocytes, and antithrombotic action. *Biochem Med Metab Biol* **35,** 101–114 (1986).
73. Prabhakar, G., Vona-Davis, L., Murray, D., Lakhani, P. & Murray, G. Phosphocreatine restores high-energy phosphates in ischemic myocardium: Implication for off-pump cardiac revascularization. *J Am Coll Surg* **197,** 786–791 (2003).
74. Zhang, W., Zhang, H. & Xing, Y. Protective Effects of Phosphocreatine Administered Post-Treatment Combined With Ischemic Post-Conditioning on Rat Hearts With Myocardial Ischemia/Reperfusion Injury. *J Clin Med Res* **7,** 242–247 (2015).
75. Qaed, E., Wang, J., Almoiliqy, M., Song, Y., Liu, W., Chu, P., Alademi, S., Alademi, M., Li, H., Alshwmi, M., Al-Azab, M., Ahsan, A., Mahdi, S., Han, G., Niu, M., Ali, A., Shopit, A., Wang, H., Li, X., Qaid, A., Ma, X., Li, T., Peng, J., Ma, J., Zhang, J. & Tang, Z. Phosphocreatine improves cardiac dysfunction by normalizing mitochondrial respiratory function through JAK2/STAT3 signaling pathway in vivo and in vitro. *Oxid Med Cell Longev* **2019,** (2019).
76. Wang, C. X., Guo, J. J., Di, A. J., Zhu, Y., Han, W. M., Cheng, A. R., Li, C., Si, R. C., Lan, T. S., Zhang, R., Liu, H. L. & Yan, G. L. The Protective Effect of Cx43 Protein-Mediated Phosphocreatine on Myocardial Ischemia/Reperfusion Injury. *Cardiol Res Pract* **2021,** (2021).
77. Cheon, J. H., Kim, S. Y., Son, J. Y., Kang, Y. R., An, J. H., Kwon, J. H., Song, H. S., Moon, A., Lee, B. M. & Kim, H. S. Pyruvate kinase M2: A novel biomarker for the early detection of acute kidney injury. *Toxicol Res* **32,** 47–56 (2016).

78. Wang, Z., Chatterjee, D., Jeon, H. Y., Akerman, M., Vander Heiden, M. G., Cantley, L. C. & Krainer, A. R. Exon-centric regulation of pyruvate kinase M alternative splicing via mutually exclusive exons. *J Mol Cell Biol* **4,** 79–87 (2012).
79. Hauck, L., Dadson, K., Chauhan, S., Grothe, D. & Billia, F. Inhibiting the Pkm2 / b-catenin axis drives in vivo replication of adult cardiomyocytes following experimental MI. *Cell Death Differ* 1398–1417 (2021). doi:10.1038/s41418-020-00669-9
80. Cheng, Y., Feng, Y., Xia, Z., Li, X. & Rong, J. ω-Alkynyl arachidonic acid promotes anti-inflammatory macrophage M2 polarization against acute myocardial infarction via regulating the cross-talk between PKM2, HIF-1α and iNOS. *BBA - Molecular and Cell Biology of Lipids* **1862,** 1595–1605 (2017).
81. TeSlaa, T., Ralser, M., Fan, J. & Rabinowitz, J. D. The pentose phosphate pathway in health and disease. *Nat Metab* **5,** 1275–1289 (2023).
82. Hauck, L., Dadson, K., Chauhan, S., Grothe, D. & Billia, F. Inhibiting the Pkm2 / b-catenin axis drives in vivo replication of adult cardiomyocytes following experimental MI. *Cell Death Differ* 1398–1417 (2021). doi:10.1038/s41418-020-00669-9
83. Cheng, Y., Feng, Y., Xia, Z., Li, X. & Rong, J. ω-Alkynyl arachidonic acid promotes anti-inflammatory macrophage M2 polarization against acute myocardial infarction via regulating the cross-talk between PKM2, HIF-1α and iNOS. *BBA - Molecular and Cell Biology of Lipids* **1862,** 1595–1605 (2017).
84. Gupte, S. A., Levine, R. J., Gupte, R. S., Young, M. E., Lionetti, V., Labinskyy, V., Floyd, B. C., Ojaimi, C., Bellomo, M., Wolin, M. S. & Recchia, F. A. Glucose-6-phosphate dehydrogenase-derived NADPH fuels superoxide production in the failing heart. *J Mol Cell Cardiol* **41,** 340–349 (2006).
85. Wang, X., Zhang, G., Dasgupta, S., Niewold, E. L., Li, C., Li, Q., Luo, X., Tan, L., Ferdous, A., Lorenzi, P. L., Rothermel, B. A., Gillette, T. G., Adams, C. M., Scherer, P. E., Hill, J. A. & Wang, Z. V. ATF4 Protects the Heart From Failure by Antagonizing Oxidative Stress. *Circ Res* **131,** 91–105 (2022).
86. Zoccarato, A., Smyrnias, I., Reumiller, C. M., Hafstad, A. D., Chong, M., Richards, D. A., Santos, C. X. C., Visnagri, A., Bromage, D. I., Zhang, X., Sawyer, G., Thompson, R. & Shah, A. M. NRF2 activation in the heart induces glucose metabolic reprogramming and mediates cardioprotection via upregulation of the pentose phosphate pathway. *bioRxiv* 2023.05.12.540342 (2023). doi:10.1101/2023.05.12.540342
87. Zhou, H. L., Hausladen, A., Anand, P., Rajavel, M., Stomberski, C. T., Zhang, R., Premont, R. T., Greenlee, W. J., van den Akker, F. & Stamler, J. S. Identification of a Selective SCoR2 Inhibitor That Protects Against Acute Kidney Injury. *J Med Chem* **66,** 5657–5668 (2023).
88. Garg, S. S. & Gupta, J. Polyol pathway and redox balance in diabetes. *Pharmacol Res* **182,** 106326 (2022).
89. Touster, O., Reynolds, V. & Hutcheson, R. The reduction of L-xylulose to xylitol by guinea pig liver mitochondria. *J Biol Chem* **221,** 697–709 (1956).
90. Touster, O. & Harwell, S. The isolation of L-arabitol from pentosuric urine. *J Biol Chem* **230,** 1031–1041 (1958).
91. Rice, T., Zannini, E., K Arendt, E. & Coffey, A. A review of polyols - biotechnological production, food applications, regulation, labeling and health effects. *Crit Rev Food Sci Nutr* **60,** 2034–2051 (2020).

92. Monedero, V., Pérez-Martínez, G. & Yebra, M. J. Perspectives of engineering lactic acid bacteria for biotechnological polyol production. *Appl Microbiol Biotechnol* **86,** 1003–1015 (2010).
93. Hootman, K. C., Trezzi, J. P., Kraemer, L., Burwell, L. S., Dong, X., Guertin, K. A., Jaeger, C., Stover, P. J., Hiller, K. & Cassano, P. A. Erythritol is a pentose-phosphate pathway metabolite and associated with adiposity gain in young adults. *Proc Natl Acad Sci U S A* **114,** E4233–E4240 (2017).
94. Schlicker, L., Szebenyi, D. M. E., Ortiz, S. R., Heinz, A., Hiller, K. & Field, M. S. Unexpected roles for ADH1 and SORD in catalyzing the final step of erythritol biosynthesis. *Journal of Biological Chemistry* **294,** 16095–16108 (2019).
95. Hiele, M., Ghoos, Y., Rutgeerts, P. & Vantrappen, G. Metabolism of erythritol in humans: Comparison with glucose and lactitol. *British Journal of Nutrition* **69,** 169–176 (1993).
96. Boyle, L., Wamelink, M. M. C., Salomons, G. S., Roos, B., Pop, A., Dauber, A., Hwa, V., Andrew, M., Douglas, J., Feingold, M., Kramer, N., Saitta, S., Retterer, K., Cho, M. T., Begtrup, A., Monaghan, K. G., Wynn, J. & Chung, W. K. Mutations in TKT are the cause of a syndrome including short stature, developmental delay, and congenital heart defects. *Am J Hum Genet* **98,** 1235–1242 (2016).
97. Verhoeven, N. M., Huck, J. H. J., Roos, B., Struys, E. A., Salomons, G. S., Douwes, A. C., Van der Knaap, M. S. & Jakobs, C. Transaldolase deficiency: Liver cirrhosis associated with a new inborn error in the pentose phosphate pathway. *Am J Hum Genet* **68,** 1086–1092 (2001).
98. Hoshino, S., Manya, H., Imae, R., Kobayashi, K., Kanagawa, M. & Endo, T. Endogenous reductase activities for the generation of ribitol-phosphate, a CDP-ribitol precursor, in mammals. *The Journal of Biochemistry* mvad115 (2023). doi:10.1093/jb/mvad115
99. Castillo, O. A., Herrera, G., Manriquez, C., Rojas, A. F. & González, D. R. Pharmacological inhibition of s-nitrosoglutathione reductase reduces cardiac damage induced by ischemia–reperfusion. *Antioxidants* **10,** (2021).
100. Grimmett, Z. W., Venetos, N. M., Premont, R. T. & Stamler, J. S. GSNOR regulates cardiomyocyte differentiation and maturation through protein S-nitrosylation. *Journal of Cardiovascular Aging* **1,** 1–5 (2021).
101. Hatzistergos, K. E., Paulino, E. C., Dulce, R. A., Takeuchi, L. M., Bellio, M. A., Kulandavelu, S., Cao, Y., Balkan, W., Kanashiro-Takeuchi, R. M. & Hare, J. M. S-nitrosoglutathione reductase deficiency enhances the proliferative expansion of adult heart progenitors and myocytes post myocardial infarction. *J Am Heart Assoc* **4,** (2015).
102. Perone, F. & Lembo, G. Thioredoxin-1: A cardioprotector against stress. *Cardiovasc Res* **116,** 1654–1655 (2020).
103. Tao, L., Gao, E., Bryan, N. S., Qu, Y., Liu, H. R., Hu, A., Christopher, T. A., Lopez, B. L., Yodoi, J., Koch, W. J., Feelisch, M. & Ma, X. L. Cardioprotective effects of thioredoxin in myocardial ischemia and the reperfusion role of S-nitrosation. *Proc Natl Acad Sci U S A* **101,** 11471–11476 (2004).
104. Anand, P., Hausladen, A., Wang, Y. J., Zhang, G. F., Stomberski, C., Brunengraber, H., Hess, D. T. & Stamler, J. S. Identification of S-nitroso-CoA reductases that regulate protein S-nitrosylation. *Proc Natl Acad Sci U S A* **111,** 18572–18577 (2014).
105. Shioura, K. M., Geenen, D. L. & Goldspink, P. H. Sex-related changes in cardiac function following myocardial infarction in mice. *Am J Physiol Regul Integr Comp Physiol* **295,** 528–534 (2008).

106. Kam, K. W. L., Qi, J. S., Chen, M. & Wong, T. M. Estrogen Reduces Cardiac Injury and Expression of β1-Adrenoceptor upon Ischemic Insult in the Rat Heart. *Journal of Pharmacology and Experimental Therapeutics* **309,** 8–15 (2004).
107. Bridgman, P., Aronovitz, M. A., Kakkar, R., Oliverio, M. I., Coffman, T. M., Rand, W. M., Konstam, M. A., Mendelsohn, M. E. & Patten, R. D. Gender-specific patterns of left ventricular and myocyte remodeling following myocardial infarction in mice deficient in the angiotensin II type 1a receptor. *Am J Physiol Heart Circ Physiol* **289,** 586–592 (2005).
108. Brower, G. L., Gardner, J. D. & Janicki, J. S. Gender mediated cardiac protection from adverse ventricular remodeling is abolished by ovariectomy. *Mol Cell Biochem* **251,** 89–95 (2003).
109. Korte, T., Fuchs, M., Arkudas, A., Geertz, S., Meyer, R., Gardiwal, A., Klein, G., Niehaus, M., Krust, A., Chambon, P., Drexler, H., Fink, K. & Grohé, C. Female mice lacking estrogen receptor β display prolonged ventricular repolarization and reduced ventricular automaticity after myocardial infarction. *Circulation* **111,** 2282–2290 (2005).
110. Pullen, A. B., Kain, V., Serhan, C. N. & Halade, G. V. Molecular and cellular differences in cardiac repair of male and female mice. *J Am Heart Assoc* **9,** (2020).
111. Zhang, R., Hess, D. T., Reynolds, J. D. & Stamler, J. S. Hemoglobin S-nitrosylation plays an essential role in cardioprotection. *Journal of Clinical Investigation* **126,** 4654–4658 (2016).
112. Forrester, M. T., Thompson, J. W., Foster, M. W., Nogueira, L., Moseley, M. A. & Stamler, J. S. Proteomic analysis of S-nitrosylation and denitrosylation by resin-assisted capture. *Nat Biotechnol* **27,** 557–559 (2009).
113. Seth, P., Hausladen, A., Premont, R. T. & Stamler, J. S. Protocol for preparing Thiopropyl-Sepharose resin used for capturing S-nitrosylated proteins. *STAR Protoc* **4,** (2023).
114. Eng, J. K., McCormack, A. L. & Yates, J. R. An approach to correlate tandem mass spectral data of peptides with amino acid sequences in a protein database. *J Am Soc Mass Spectrom* **5,** 976–989 (1994).
115. Huttlin, E. L., Jedrychowski, M. P., Elias, J. E., Goswami, T., Rad, R., Beausoleil, S. A., Villén, J., Haas, W., Sowa, M. E. & Gygi, S. P. A tissue-specific atlas of mouse protein phosphorylation and expression. *Cell* **143,** 1174–1189 (2010).
116. Elias, J. E. & Gygi, S. P. Target-decoy search strategy for increased confidence in large-scale protein identifications by mass spectrometry. *Nat Methods* **4,** 207–214 (2007).
117. Chen, Q., Kirk, K., Shurubor, Y. I., Zhao, D., Arreguin, A. J., Shahi, I., Valsecchi, F., Primiano, G., Calder, E. L., Carelli, V., Denton, T. T., Beal, M. F., Gross, S. S., Manfredi, G. & D'Aurelio, M. Rewiring of Glutamine Metabolism Is a Bioenergetic Adaptation of Human Cells with Mitochondrial DNA Mutations. *Cell Metab* **27,** 1007-1025.e5 (2018).

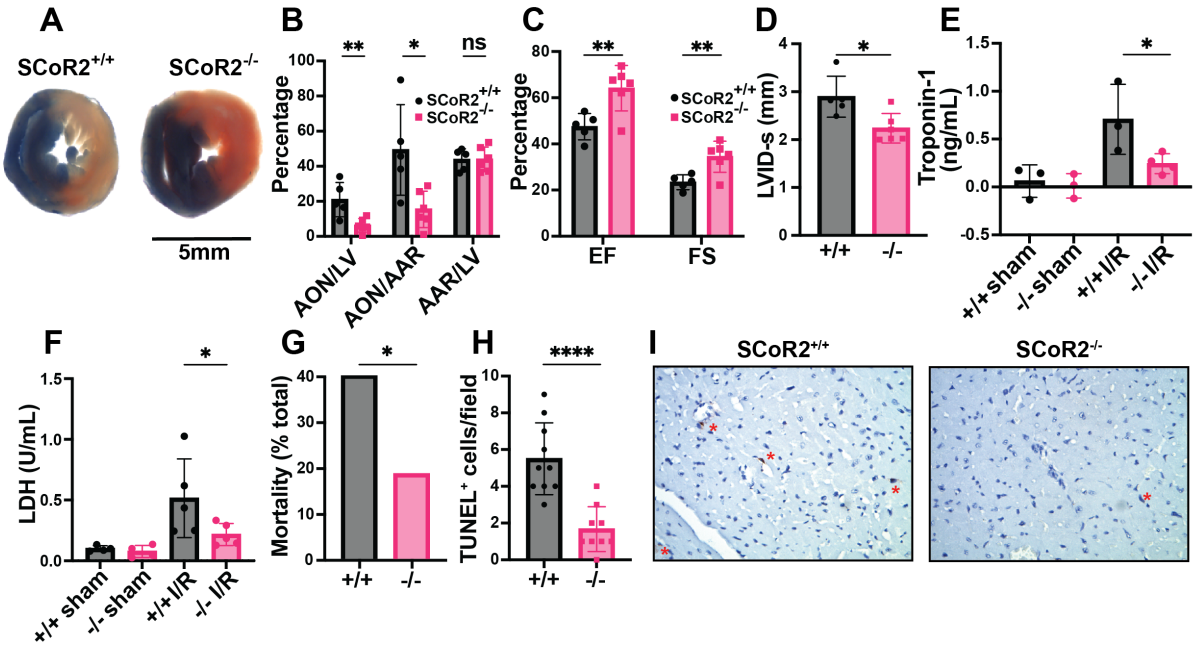

Figure 1. Knockout of SCoR2 protects from myocardial injury. (**A**) Representative myocardial infarct staining after I/R in SCoR2$^{+/+}$ (+/+) and SCoR2$^{-/-}$ (–/–) mice, taken from the same anatomical plane. Infarcted necrotic tissue is white, the area at risk is red, and tissue with normal perfusion is dark blue. (**B**) Quantification of the myocardial infarct size after I/R injury (24-hour reperfusion). AON (area of necrosis) is expressed as a percentage of the LV (left ventricle) and AAR (area at risk). (**C**) Quantification of left ventricular function after I/R injury (24-hour reperfusion). Ejection fraction (EF) and fractional shortening (FS) were determined by echocardiography. (**D**) Left ventricular internal diameter at end systole (LVID-s) was measured in SCoR2$^{+/+}$ and SCoR2$^{-/-}$ mice after I/R injury (24-hour reperfusion). (A-D): N=5 +/+ , 6 –/– mice. (**E**) Serum Troponin-1 concentration in +/+ and –/– mice after I/R injury (4-hour reperfusion); N=3-4 mice/condition. (**F**) Serum LDH concentration in +/+ and –/– mice after I/R injury (4-hour reperfusion) normalized to +/+ sham; N=4-5 mice/condition. (**G**) Quantification of post-MI survival at 4 hr post-reperfusion in –/– (N=27) and +/+ (N=30) mice. (**H, I**) Quantification of TUNEL^{+} (apoptotic) nuclei in post-MI +/+ vs. –/– myocardium at 4 hr post-reperfusion (N=3 each), with representative images in (I). Red asterisks indicate TUNEL^{+} nuclei. Significance in

(B-D) assessed by two-tailed Student's t-test, in (E) by one-tailed Mann-Whitney test, in (F) by one-tailed Student's t-test, in (G) by one-sided chi-squared test, and in (H) by two-tailed Student's t-test; * $p < 0.05$, ** $p < 0.01$, ns = not significant.

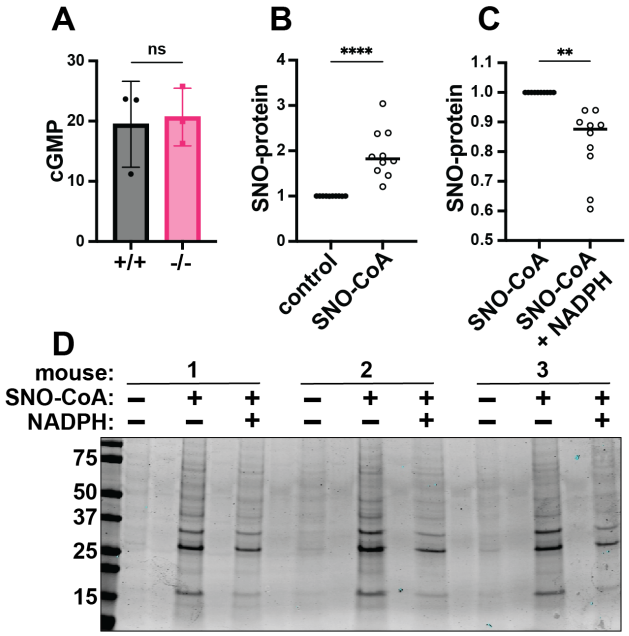

Figure 2. SCoR2 regulates protein S-nitrosylation in the mouse heart. (**A**) cGMP (pmol/mg total protein) in SCoR2$^{+/+}$ (+/+) and SCoR2$^{-/-}$ (–/–) mouse heart lysate post-I/R (1hr reperfusion) as assessed by ELISA; N=3 mouse hearts per group. (**B**) SNO-CoA (60µM) added to +/+ mouse heart lysate (1mg/mL) for 10min increases protein S-nitrosylation as assessed by SNORAC and Coomassie blue staining, shown as fold increase relative to control after normalization to total protein; N=10 +/+ mouse hearts per group. (**C**) In the presence of 100µM NADPH (required for SCoR2 activity), cardiac protein S-nitrosylation is reduced, shown as fold decrease relative to SNO-CoA normalized to total protein; N=10 +/+ mouse hearts per group. (**D**) Representative Coomassie-stained SDS/PAGE gel displaying SNO-proteins isolated by SNORAC following incubation of mouse heart extract with SNO-CoA alone or in combination with NADPH, as quantified in (B) and (C). Significance in (A) assessed by two-tailed Mann-Whitney test, and in (B, C) by ratio paired one-tailed Student's t-test. * $p \leq 0.05$, ** $p \leq 0.01$, *** $p \leq 0.001$, **** $p \leq 0.0001$.

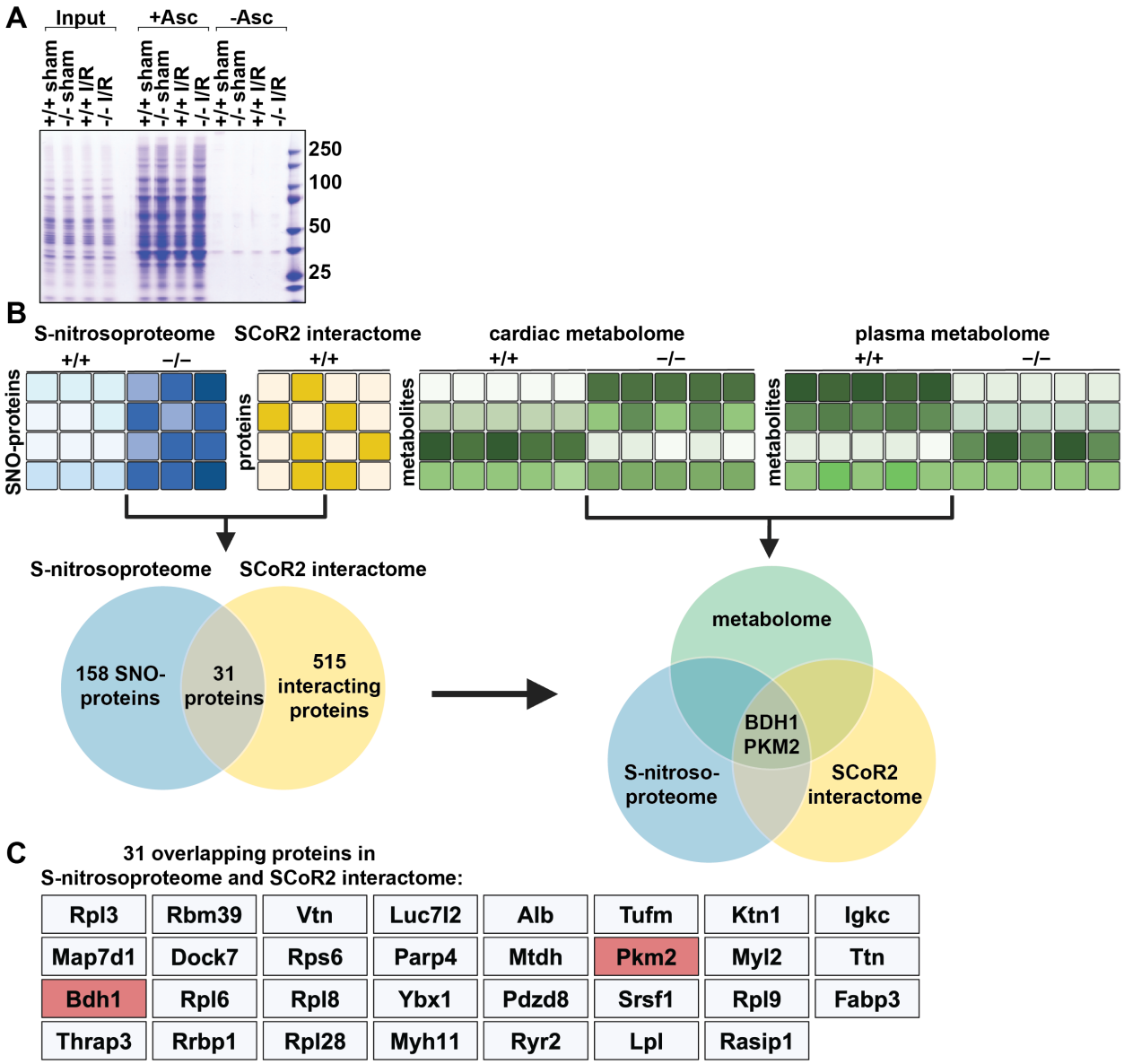

Figure 3. A combined multi-omics approach identifies SCoR2-regulated SNO-proteins and metabolic pathways responsible for widespread metabolic reprogramming. (A) S-nitrosylated proteins in heart of SCoR2$^{+/+}$ (+/+) and SCoR2$^{-/-}$ (–/–) mice post-I/R vs sham. Representative Coomassie-stained SDS/PAGE gel displaying SNO-proteins isolated by SNORAC using hearts of +/+ and –/– mice subjected to either sham operation or I/R (4hr reperfusion). Ascorbate was omitted from the SNORAC assay (-Asc) as a specificity control. (**B**): Three coordinated screens in +/+ vs. –/– mouse heart tissue, i.e. (1) SNORAC/MS (SCoR2-dependent S-nitrosoproteome 4

h after I/R, elevated >1.2-fold in –/– vs +/+) (Table S1; N=3), (2) SCoR2 co-IP interactome (Table S1; N=4), and (3) untargeted metabolomic screening in heart and plasma (Table S2; N=5 per condition), converge on the proteins BDH1 and PKM2 as SCoR2 substrate SNO-proteins in the heart which alter relevant cardioprotective metabolic pathways. (**C**) Full list of 31 overlapping proteins identified in both screens (1) and (2) i.e., the cardiac SCoR2-dependent S-nitrosoproteome and the cardiac SCoR2 interactome. Image created with Biorender.com.

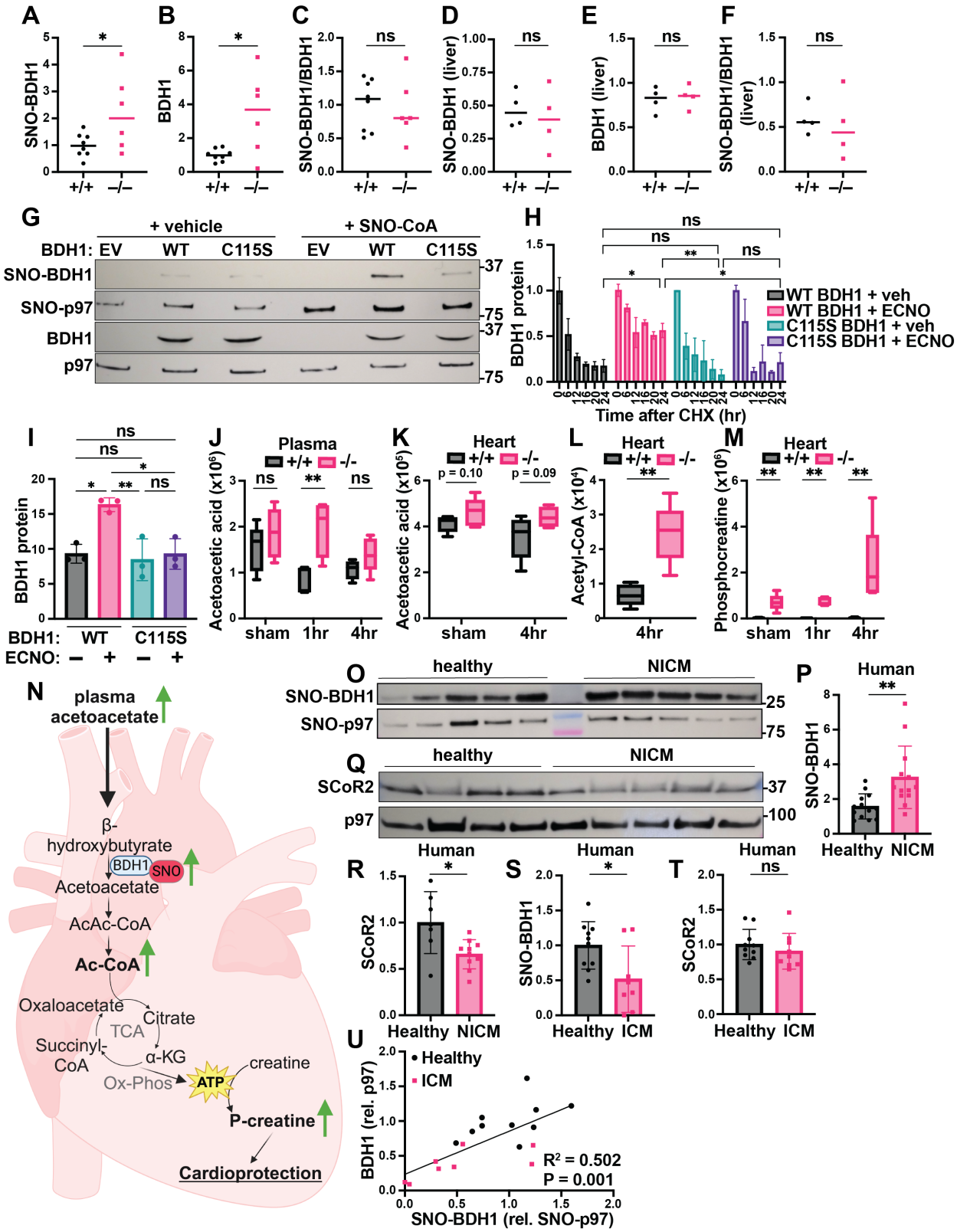

Figure 4. SCoR2 regulates S-nitrosylation of BDH1 at Cys[115], impacting ketolytic energy availability. (**A-C**): Quantification of SNO-BDH1 (A) and total BDH1 (B), relative to p97 ATPase

loading control and to each other (C), in mouse heart (4 hr reperfusion); N=8 SCoR2$^{+/+}$ (+/+), N=6 SCoR2$^{-/-}$ (–/–). Representative Western blots shown in Fig. S3A. (**D-F**) Quantification of SNO-BDH1 (D) and total BDH1 (E), relative to p97 ATPase loading control and to each other (F), in mouse liver (1 hr reperfusion); N=4 each. (**G**): HEK293 cells transfected with empty vector (EV), WT or C115S BDH1 were treated with 250µM SNO-CoA or vehicle for 10 min, followed by SNORAC and blotted for SNO-BDH1 and BDH1, together with loading controls SNO-p97 ATPase and input p97 ATPase. Representative of 4 independent experiments. (**H, I**): CHX pulse-chase assay, in which HEK293 cells transfected with V5-tagged BDH1 were treated with 100µM ECNO or vehicle, in addition to 100µg/mL CHX for 6-24hr. BDH1 protein expression was quantified relative to t=0 (pre-CHX) in (H), and area under the curve (AUC) quantified in (I); N=3 samples/group. (**J-M**): Metabolites corresponding to ketolytic energy availability in mouse heart and plasma subjected to sham or I/R injury (1hr or 4hr reperfusion), quantified as ion abundance by LC/MS-based untargeted metabolite profiling: (J) plasma acetoacetic acid, (K) heart acetoacetic acid, (L) heart acetyl-CoA, (M) heart phosphocreatine. N=5 mice per condition per genotype. (**N**): Model depicting effect of SCoR2 deletion on cardiac ketone body metabolism in SCoR2$^{-/-}$ mice. (**O-R**): Human heart samples (IRB# Pro00005621, N=13 with diagnosis of non-ischemic cardiomyopathy (NICM) and N=13 without known cardiac pathophysiology (healthy)) subjected to SNORAC measuring SNO-BDH1 expression relative to loading control (SNO-p97 ATPase), representative SNORAC shown in (O), quantification in (P). (**Q, R**) SCoR2 protein expression in human heart samples (N=7 healthy, N=10 NICM from same cohort), as determined by Western blot relative to p97 ATPase (representative image in (Q), quantified in (R)). (**S-U**): Human heart samples (IRB# Pro00005621, N=8-9 with diagnosis of ischemic cardiomyopathy (ICM; pink) and N=10 without known cardiac pathophysiology (healthy; black)) subjected to SNORAC measuring SNO-BDH1 (S) or Western blot measuring SCoR2 relative to loading control (SNO-p97 ATPase

or p97, respectively). Representative SNORAC/Western blot gels shown in Fig. S3G,H. Correlation of SNO-BDH1 (normalized to SNO-p97) vs. BDH1 (normalized to p97) expression in healthy (N=10) and ICM (N=8) heart was assessed by simple linear regression in (U). Statistical significance in (A-C) determined by two-tailed Student's t-test; (D-F) determined by two-tailed Mann-Whitney test; (H) determined by two-way ANOVA with Tukey's multiple comparisons test; (I) determined by one-way ANOVA with Tukey's multiple comparisons test; (J-L) determined by multiple independent Student's t-tests performed between genotypes in each condition; (M,P) determined by two-tailed Mann-Whitney test; (R-T) determined by Student's t-test; (U) determined by simple linear regression performed to identify SNO-BDH1 vs. BDH1 relationship. R^2 and p-value show the goodness of fit of the regression model and significance of slope difference from zero, respectively. * $p \leq 0.05$, ** $p \leq 0.01$, *** $p \leq 0.001$, **** $p \leq 0.0001$, ns = not significant.

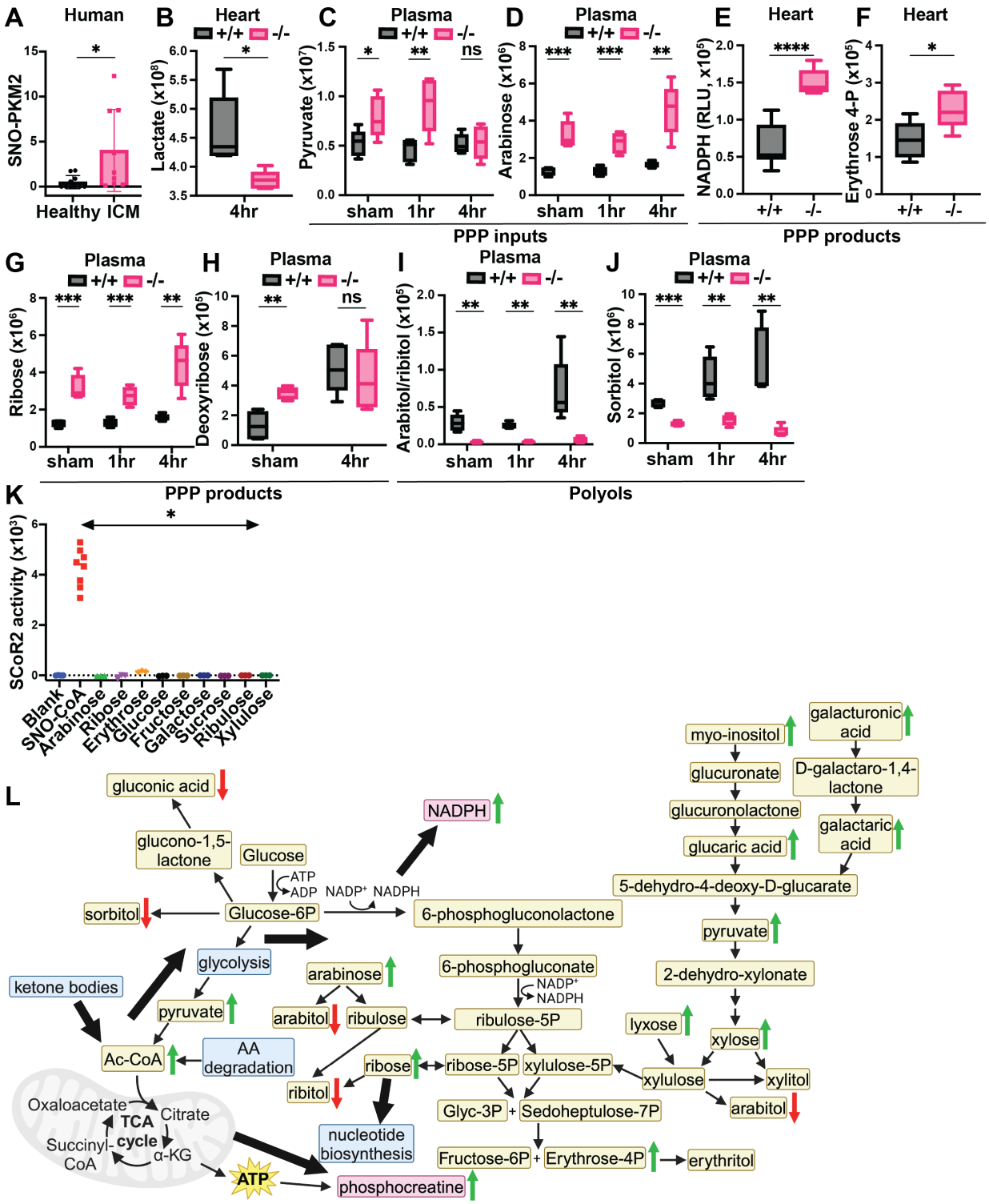

Figure 5. SCoR2 regulates carbohydrate metabolism, including polyols, to provide antioxidative protection from injury via the pentose phosphate shunt pathway (PPP). (A): Human heart samples (IRB# Pro00005621, N=9 with diagnosis of ischemic cardiomyopathy

(ICM) and N=10 without known cardiac pathophysiology (healthy)) subjected to SNORAC measuring SNO-PKM2 relative to loading control (SNO-p97 ATPase). Representative SNORAC/Western blot gels shown in Fig. S3G,H. (**B-J**): Metabolites quantified by ion abundance in SCoR2$^{+/+}$ (+/+) and SCoR2$^{-/-}$ (–/–) mouse heart and plasma by LC/MS-based untargeted metabolite profiling; N=5 each condition. (B) Heart lactate. (C-K) Metabolites organized by relationship to the PPP, as inputs (C,D), products (E-H), or polyol compounds that are categorized as downstream end products of the PPP (I,J). NADPH measured in heart lysate after 2 hr reperfusion, erythrose 4-phosphate measured after 4 hr reperfusion. (**K**): Recombinant SCoR2 activity quantified via NADPH consumption by spectrophotometer in the presence of canonical substrate (100μM SNO-CoA) or carbohydrates (1mM); [SCoR2] = 186nM, [NADPH] = 100μM. Results presented as specific activity of SCoR2 (μM substrate consumed/min/mg protein). Assay performed in triplicate. (**L**): Summary model showing SCoR2-mediated regulation of carbohydrate metabolism, including PPP and polyol compounds, to generate NADPH and phosphocreatine in the mouse heart. Green arrows indicate pathway upregulation in the absence of SCoR2 and red arrows indicate downregulation. Blue boxes indicate metabolic pathways, tan boxes indicate metabolites, and pink boxes indicate metabolites of particular significance. Thick black arrows indicate directions of SCoR2-regulated metabolic changes. Image created with Biorender.com. Statistical significance in (A) determined by Student's t-test; (B-H,J) determined by multiple independent Student's t-tests performed between genotypes in each condition; (I) determined by two-tailed Mann-Whitney test; (K) determined by two-tailed Mann-Whitney test between SNO-CoA condition and each carbohydrate condition (N = 3-8 independent replicates per condition). * $p \leq 0.05$, ** $p \leq 0.01$, *** $p \leq 0.001$, **** $p \leq 0.0001$.

Metabolite	Organ	SCoR2$^{+/+}$			SCoR2$^{-/-}$		
		sham	MI (1hr)	MI (4hr)	sham	MI (1hr)	MI (4hr)
Galactaric acid	heart	4.88E+04 +/- 2.14E+04	7.08E+04 +/- 3.62E+04	2.16E+04 +/- 1.64E+04	1.09E+05 +/- 2.37E+04	1.17E+05 +/- 2.44E+04	2.84E+05 +/- 2.13E+05
Galactaric acid	plasma	4.90E+05 +/- 1.83E+05	3.83E+05 +/- 8.86E+04	8.05E+05 +/- 2.16E+05	6.14E+06 +/- 1.84E+06	5.82E+06 +/- 2.11E+06	1.42E+07 +/- 6.43E+06
Galacturonic acid	heart	4.70E+04 +/- 4.03E+04	5.53E+04 +/- 2.38E+04	1.24E+05 +/- 2.36E+04	3.71E+05 +/- 1.63E+05	3.47E+05 +/- 8.03E+04	9.85E+05 +/- 5.72E+05
Galacturonic acid	plasma	6.06E+07 +/- 2.18E+07	5.32E+07 +/- 8.19E+06	1.54E+08 +/- 3.76E+07	5.05E+08 +/- 9.52E+07	4.42E+08 +/- 7.53E+07	8.55E+08 +/- 2.53E+08
Glucaric acid	heart	3.08E+05 +/- 1.36E+05	3.31E+05 +/- 9.75E+04	4.46E+05 +/- 1.74E+05	9.58E+06 +/- 4.84E+06	9.93E+06 +/- 2.53E+06	3.35E+07 +/- 2.68E+07
Glucaric acid	plasma	2.13E+06 +/- 6.93E+05	2.26E+06 +/- 7.27E+05	5.92E+06 +/- 1.28E+06	1.81E+08 +/- 3.10E+07	1.66E+08 +/- 4.77E+07	2.68E+08 +/- 9.96E+07
Xylose	plasma	1.36E+06 +/- 1.95E+05	1.35E+06 +/- 2.51E+05	1.68E+06 +/- 1.61E+05	3.37E+06 +/- 7.05E+05	2.91E+06 +/- 5.66E+05	4.70E+06 +/- 1.35E+06
Lyxose	plasma	1.08E+06 +/- 1.69E+05	1.10E+06 +/- 1.88E+05	1.39E+06 +/- 1.71E+05	2.84E+06 +/- 6.11E+05	2.41E+06 +/- 4.26E+05	4.02E+06 +/- 1.20E+06

Table 1. **Input metabolites to the PPP via xylulose.** Relative quantity, quantified in mean ion abundance +/- standard deviation by LC/MS-based untargeted metabolomic platform, as described in the Methods.

Supplementary Materials

Figure S1: Characterization of SCoR2$^{-/-}$ mice at baseline and 24 hr post-MI.

Figure S2: Characterization of SCoR2 and protein S-nitrosylation in SCoR2$^{-/-}$ mice.

Figure S3: Characterization of BDH1 S-nitrosylation at the conserved SNO site Cys^{115}.

Table S1 (Excel file): SCoR2-dependent cardiac S-nitrosoproteome and SCoR2 interactome

Table S2 (Excel file): SCoR2-dependent cardiac and plasma metabolome

Table S3 (Excel file): Statistical values for all quantitative experimental results

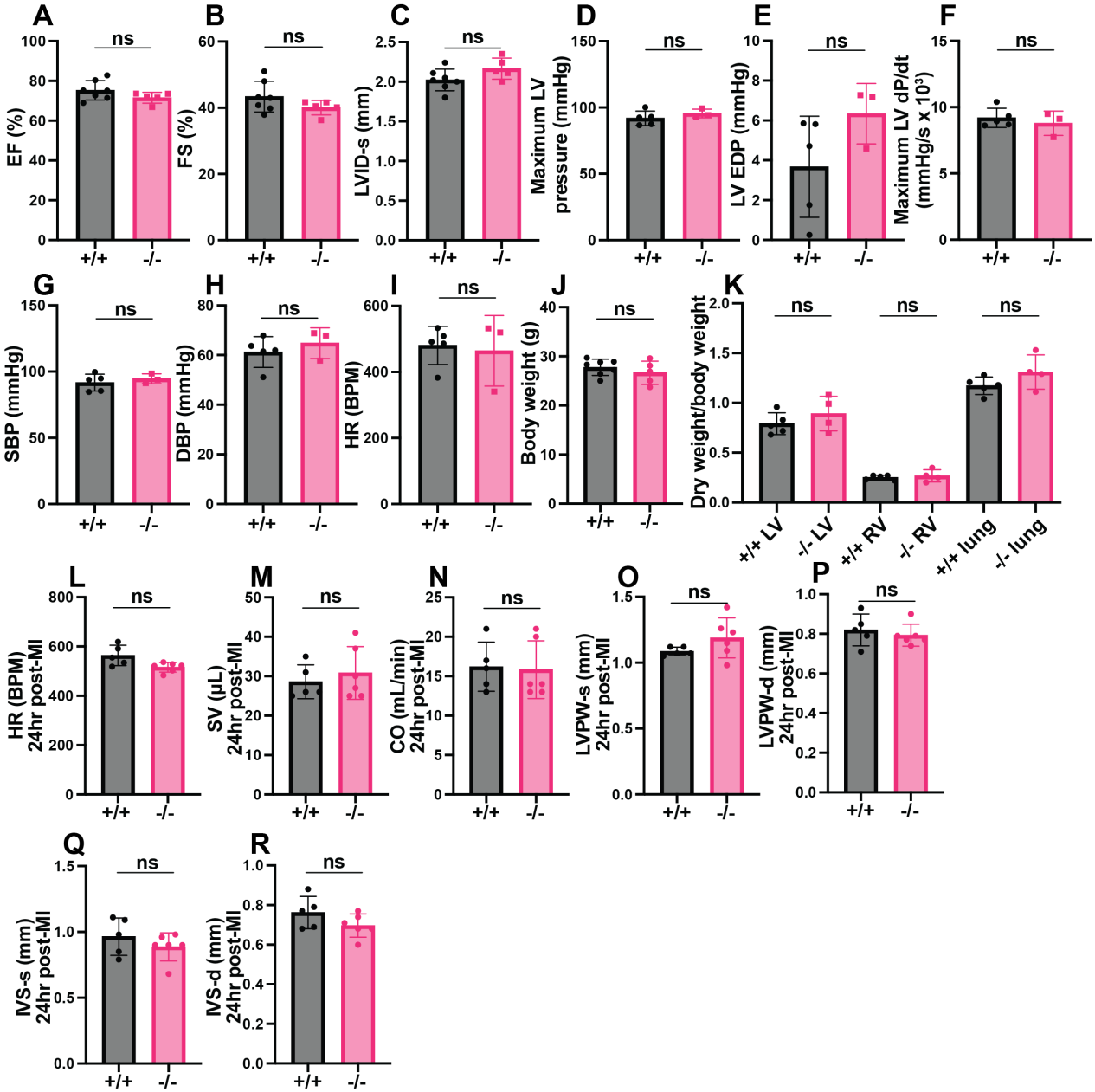

Figure S1. Characterization of SCoR2$^{-/-}$ mice at baseline and 24 hours post-MI. (**A-K**) Quantification of left ventricular contractile function (**A-F**), blood pressure (**G,H**), heart rate (**I**), and weight (**J,K**) in uninjured SCoR2$^{+/+}$ (+/+) and SCoR2$^{-/-}$ (–/–) mice at baseline. Ejection fraction (EF; (A)), fractional shortening (FS; (B)), left ventricular diameter at end systole (LVID-s; (C)), maximum LV pressure (D), left ventricular end diastolic pressure (LV EDP; (E)), maximum change in LV pressure over time (LV dP/dt; (F)), systolic blood pressure (SBP; (G)), diastolic blood pressure (DBP; (H)) and heart rate (HR; (I)) were determined by echocardiography

in N=3-7 uninjured +/+ and –/– mice. Body weight and ratio of left ventricle (LV), right ventricle (RV), and lung dry weight to body weight were quantified in N=4-5 +/+ and –/– mice in (J) and (K), respectively. At 24 hr post-MI, heart rate (HR; (**L**)) and left ventricular parameters (stroke volume (SV; (**M**)), cardiac output (CO; (**N**)), left ventricular posterior wall at end systole/diastole (LVPW-s (**O**), LVPW-d; (**P**)) and interventricular septal at end systole/diastole (IVS-s (**Q**), IVS-d (**R**))) were determined by echocardiography in N=5-6 +/+ and –/– mice. Statistical significance in (A-R) was determined by two-tailed Mann-Whitney test; ns = not significant.

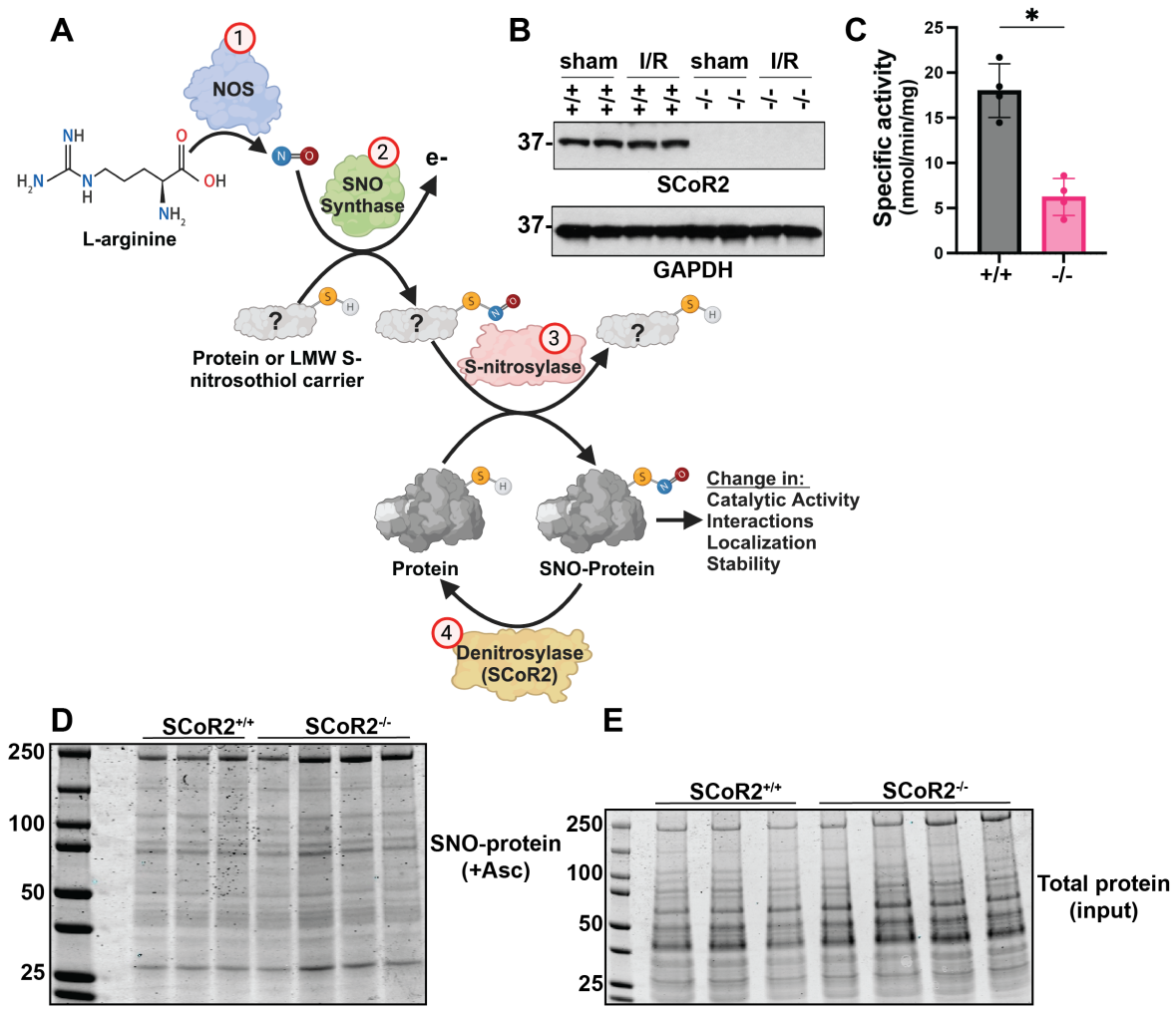

Figure S2. Characterization of SCoR2 and protein S-nitrosylation in SCoR2$^{-/-}$ mice. (**A**) Protein S-nitrosylation is regulated by four distinct classes of enzymes; NOS enzymes synthesize NO from L-arginine (1), SNO synthase enzymes produce S-nitrosothiols (SNOs) from NO (2), S-nitrosylase (aka transnitrosylase) enzymes transfer SNO to target proteins to regulate activity, interactions, localization or stability (3), denitrosylase enzymes (such as SCoR2) remove SNO from substrate proteins (4). Image created with Biorender.com. (**B**) Representative Western blot showing expression of SCoR2 in hearts of +/+ and –/– mice after sham or ischemia-reperfusion (I/R) surgery. N=4 mice per genotype. (**C**) NADPH-dependent SNO-CoA reductase activity measured in heart extracts from healthy untreated +/+ and –/– mice; N=4 mice per genotype. (**D,**

E) SNO-proteins identified via SNORAC from heart tissue isolated from healthy untreated +/+ (N=3) and –/– (N=4) mice. SNO-proteins shown in +Asc gel (D), total protein identified via Coomassie staining in input gel (E). Statistical significance in (C) determined by two-tailed Mann-Whitney test; * $p \leq 0.05$.

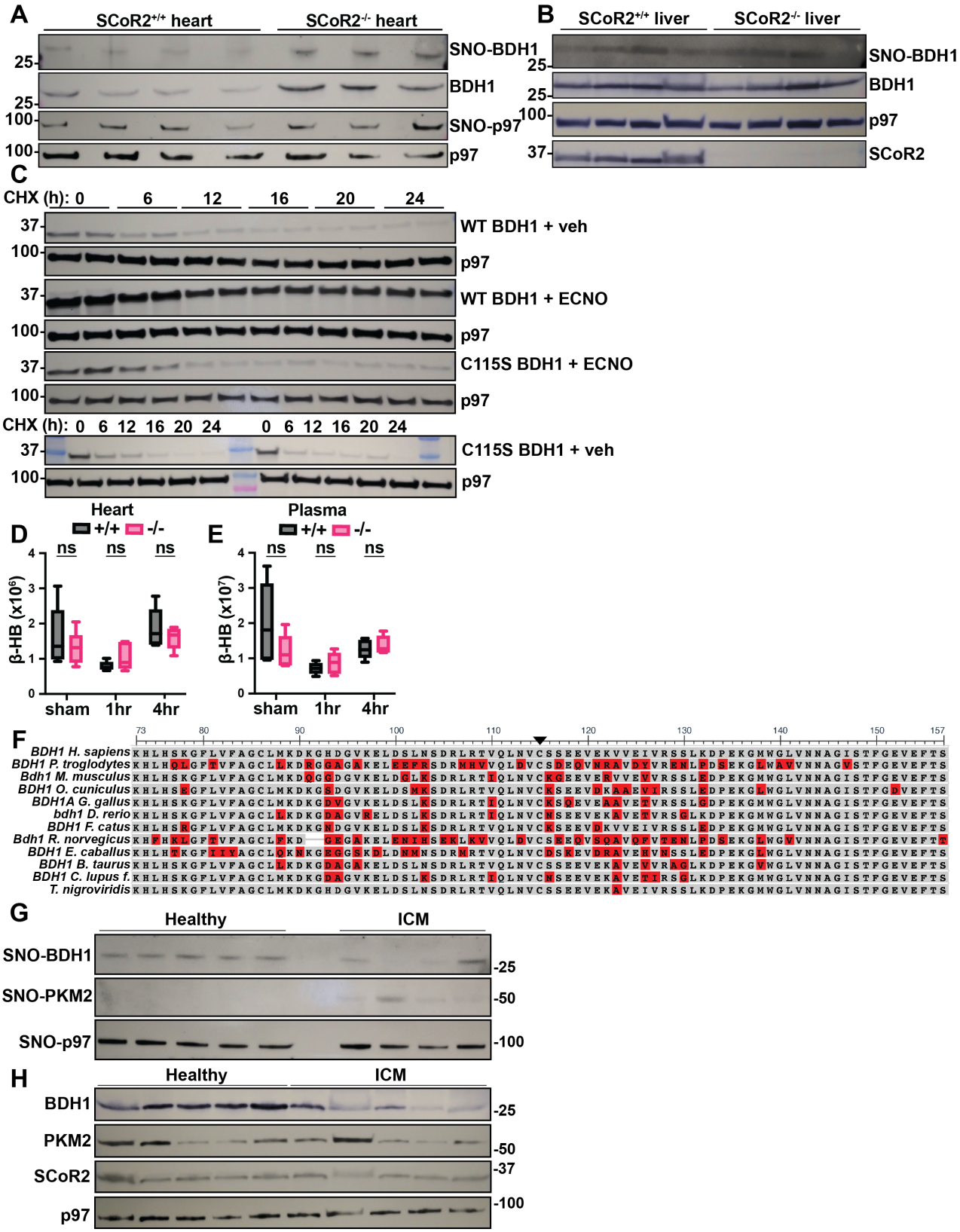

Figure S3. Characterization of BDH1 S-nitrosylation at conserved SNO site Cys[115]. (A)

Representative gel from SNORAC measuring SNO-BDH1 and Western blot measuring total BDH1, relative to p97 ATPase loading control, in mouse heart (4 hr reperfusion), quantified in Fig. 4A-C. (**B**) SNO-BDH1 assessed by SNORAC in SCoR2$^{+/+}$ (+/+) and SCoR2$^{-/-}$ (–/–) liver tissue (N=4 each) from mice (1hr reperfusion), quantified in Fig. 4D-F. (**C**) Representative Western blot, quantified in Fig. 4H,I, denoting a CHX pulse-chase assay, in which HEK293 cells transfected with V5-tagged BDH1 were treated with 100µg/mL CHX to block new protein synthesis, together with 100µM ECNO or vehicle, with samples collected at 6-24hr. Duplicates are shown by treatment condition. (**D,E**) Beta-hydroxybutyrate (β-HB) quantified as ion abundance in +/+ and –/– mouse heart and plasma by LC/MS-based untargeted metabolite profiling, N=5 mice per condition per genotype. (**F**) Sequences of BDH1, or protein product of closest homology, from selected species aligned with constraint-based multiple alignment tool (COBALT); red color shows differences from the *H. sapiens* BDH1 sequence. Cys^{115} is indicated by black arrow. *T. nigroviridis* protein product ID is CAG04267. (**G,H**) Representative gel from SNORAC assessing SNO-BDH1 and SNO-PKM2 expression relative to SNO-p97 ATPase loading control (G) and from Western blot assessing BDH1, PKM2, and SCoR2 expression relative to p97 ATPase loading control (H) in human hearts without (N=10) and with (N=8-9) diagnosis of ischemic cardiomyopathy (ICM) (IRB # Pro00005621). Statistical significance in (D, E) determined by independent Student's t-tests performed between genotypes at each time-point.